"*Oh no love! you're not alone*"

-David Bowie
"Rock 'n' Roll Suicide"
The Rise and Fall of Ziggy Stardust and the Spiders from Mars

University of Alberta

^{69}Ga and ^{71}Ga Solid-State NMR Studies of Six-Coordinate Gallium-Oxygen Complexes

by

Brett Christopher Feland

A thesis submitted to the Faculty of Graduate Studies and Research
in partial fulfillment of the requirements for the degree of

Master of Science

Department of Chemistry

Spring 2013
Edmonton, Alberta

For my wife.

Abstract

Presented herein is a solid-state ^{71}Ga and ^{69}Ga NMR study of several six-coordinate gallium-oxygen compounds: $Ga(acac)_3$, $Ga(thd)_3$, $Ga(trop)_3$, and $(NH_4)_3[Ga(cit)_2]\cdot 4H_2O$. Spectra of stationary and magic angle spinning (MAS) samples are reported, and their electric field gradient (EFG) and chemical shift anisotropy (CSA) tensor parameters are determined at the ^{71}Ga and ^{69}Ga sites. Experimental results are complemented with density functional theory (DFT) calculations using CASTEP. Tensor parameters are compared with those of similar compounds containing other group-13 metals including ^{27}Al and ^{115}In, and periodic trends are considered. This work shows that solid-state NMR studies of gallium compounds are worthwhile and practical with modern techniques, as ^{71}Ga and ^{69}Ga NMR spectra of the chosen compounds were successfully acquired and interpreted. The potential for further studies is discussed.

Preface

The material contained within this thesis is the most recent yet-unpublished work completed during my M.Sc. degree. However, this is not the only project I have been involved with during my studies. A list of publications in which I am included as an author can be found in the first appendix of this thesis, the most prominent being my work on the colossal expansion compound $Ag_3Co(CN)_6$ which was published by the *Canadian Journal of Chemistry* in 2012. The work for this project was initiated during my undergraduate degree here at the University of Alberta, while the bulk of it was performed and completed during my M.Sc. degree.

Acknowledgements

This thesis would not be possible without the support of many individuals. First and foremost, I would like to thank my supervisor, Dr. Rod Wasylishen, for his guidance throughout all of my studies. I would also like to thank Dr. Guy Bernard, to whom I owe many beers, for his helpful advice and assistance in nearly every aspect of this thesis, from data acquisition to preparing the manuscript. In addition, his preliminary studies on several gallium compounds, as well as Dr. Rob Schurko and Dr. Fu Chen's earlier work on Group 13 metal complexes, laid the groundwork for much of this project. I would like to thank Dr. Tom Nakashima, whose expertise in quadrupolar NMR pulse sequences was extremely helpful during my experiments. Thanks also go to the rest of the SS NMR research group at the University of Alberta, Rosha Teymoori and Alexandra Palech, as well as Renée Duan, the undergraduate summer student who assisted with sample preparation throughout this project.

I am extremely grateful for the work of Dr. Victor Terskikh which was invaluable to this thesis. Victor, at the National Ultrahigh-Field NMR Facility for Solids in Ottawa, ON, Canada, acquired much of the data contained herein at 21.14 T and performed CASTEP calculations. This thesis would not be possible without his insight and helpful discussions, and the NMR facility at Ottawa is the single greatest experimental resource available to SS NMR spectroscopists in Canada.

In addition, I would like to thank Dr. Klaus Eichele and Dr. David Bryce, whose programs WSolids1 and EFGShield facilitated the analysis of data in this project. To say these tools were useful would be a gross understatement.

For funding, I would like to acknowledge the University of Alberta and NSERC. This project would not have been possible without the many resources available at the University of Alberta, and I would in particular like to thank the Analytical and Instrumentation Laboratory in the Department of Chemistry for performing elemental analyses of several of the samples studied in this investigation. Access to the 900 MHz NMR spectrometer was provided by the National Ultrahigh-Field NMR Facility for Solids in Ottawa, Canada, a national research facility funded by the Canada Foundation for Innovation, the Ontario Innovation Trust, Recherche Québec, the National Research Council of Canada, and Bruker BioSpin and managed by the University of Ottawa (www.nmr900.ca).

I would also like to thank my parents, Rod and Cindy, my sister, Katie, my grandparents, Lloyd and Eileen Feland, Aloha Douglas, and my late grandfather Les Douglas, as well as the rest of my supportive family. Thanks also to my wonderful friends, too numerous to list in full, including Brendan McDermott, Justin Kautz, Mackenzie Cooper, Eric Wasylishen, Alex Rossol, Michael Ross, and my cousin, Moe Carlson.

Lastly, and most of all, I would like to thank my beautiful wife Justine, whose love and support are more precious to me than she knows.

Table of Contents

Introduction 1

Chapter 1: Background Information and Theory 4

1.1 The NMR Hamiltonian and the Zeeman Effect 4

1.2 Chemical Shift Anisotropy and Tensor Conventions 5

1.3 Electric Field Gradients and Quadrupolar Coupling 9

1.4 ^{69}Ga and ^{71}Ga Properties 17

Chapter 2: Experimental and Computational Methods 18

2.1 Sample Preparation 18

2.2 $^{69/71}$Ga NMR General Acquisition Techniques 21

2.3 Magic Angle Spinning (MAS) 22

2.4 Broad Powder Patterns and WURST Pulses 24

2.5 Summary of NMR Experiments 25

2.6 Calculation of Theoretical Spectra 26

2.7 Computational Methods 27

Chapter 3: Results and Discussion 30

3.1 Results Overview 30

3.2 $Ga(acac)_3$ 33

3.3 $Ga(thd)_3$ 39

3.4 $Ga(trop)_3$ 45

3.5 $(NH_4)_3[Ga(cit)_2]\cdot 4H_2O$ 49

3.6 Comparison of Results 53

Chapter 4: Conclusions 56

References 58

Appendix 1: List of Publications by the Author 65

Appendix 2: Skyline Projections 66

List of Tables

Table 3.1 Summary of experimental ^{69}Ga and ^{71}Ga NMR parameters for $Ga(acac)_3$, $Ga(thd)_3$, $Ga(trop)_3$, and $(NH_4)_3[Ga(cit)_2]\cdot 4H_2O$. Some equivalent Euler angle values that generated visually identical calculated spectra are given in parenthesis. [Page 31]

Table 3.2 Summary of CASTEP calculated ^{69}Ga and ^{71}Ga NMR properties for $Ga(acac)_3$, $Ga(thd)_3$, $Ga(trop)_3$, and $(NH_4)_3[Ga(cit)_2]\cdot 4H_2O$. [Page 32]

Table 3.3 Summary NMR properties for group-13 $M(acac)_3$ complexes. [Page 54]

Table 3.4 Summary NMR properties for group-13 $M(trop)_3$ complexes. [Page 54]

Table 3.5 Summary NMR properties for group-13 $M(thd)_3$ complexes. [Page 55]

List of Figures

Figure 1.1 Calculated NMR spectra for a spin-1/2 nucleus with δ_{iso} = 0 ppm and Ω = 200 ppm. Different values of κ were used to generate each CSA powder pattern, and the corresponding Mehring notation principal components have been labelled for each spectrum. Spectra were calculated using WSolids1. [Page 8]

Figure 1.2 Calculated ^{71}Ga NMR spectra at 11.75 T for the central transition of a nucleus with a C_Q = 4.5 MHz and δ_{iso} = 0 ppm, under infinitely fast MAS (left column) and stationary (right column) conditions, with different values of η_Q. CSA effects have been neglected. Spectra were calculated using WSolids1. [Page 15]

Figure 1.3 Euler angles. The reference axis system is denoted by X, Y, and Z, while the Euler angles α, β, and γ generate the new axis system, X', Y', and Z'. [Page 16]

Figure 2.1 Local chemical structure around the gallium centre in each of the four compounds $Ga(acac)_3$, $Ga(thd)_3$, $Ga(trop)_3$, and $(NH_4)_3[Ga(cit)_2]\cdot 4H_2O$. For the citrate complex, only the local $[Ga(cit)_2]^{3-}$ ion is shown. Figures were generated using structure information from the literature.[15,17,18,20] [Page 20]

Figure 3.1 Experimental and calculated ^{71}Ga NMR spectra of $Ga(acac)_3$ under 10 kHz MAS at 21.14 T. The simulated spectrum was calculated using the parameters summarized in Table **3.1**. The peaks to either side of the central, high-intensity peak are spinning sidebands. [Page 36]

Figure 3.2 Experimental and calculated ^{71}Ga NMR spectra of stationary $Ga(acac)_3$ at 11.75 and 21.14 T. The simulated spectra were calculated using the parameters summarized in Table **3.1**, but with Ω = 17 ppm (see text). [Page 37]

Figure 3.3 Experimental and calculated ^{69}Ga NMR spectra of stationary $Ga(acac)_3$ at 11.75 and 21.14 T. The simulated spectra were calculated using the parameters summarized in Table **3.1**, but with Ω = 17 ppm (see text). [Page 38]

Figure 3.4 Experimental and calculated ^{71}Ga NMR spectra of $Ga(thd)_3$ under 18 kHz MAS at 21.14 T and 30 kHz MAS at 11.75 T. The simulated spectrum at 21.14 T was calculated using the parameters summarized in Table **3.1**, while the one at 11.75 T was calculated using C_Q = 6.47 MHz, η_Q = 0.40, and δ_{iso} = -5.0 ppm (these agree

within error). The peaks to either side of the central, high-intensity peak in each spectrum are spinning sidebands. [Page 42]

Figure 3.5 Experimental and calculated ^{71}Ga NMR spectra of stationary $Ga(thd)_3$ at 11.75 and 21.14 T. The simulated spectra were calculated using the parameters summarized in Table **3.1**. [Page 43]

Figure 3.6 Experimental and calculated ^{69}Ga NMR spectra of stationary $Ga(thd)_3$ at 11.75 and 21.14 T. The simulated spectra were calculated using the parameters summarized in Table **3.1**. [Page 44]

Figure 3.7 Experimental and calculated ^{71}Ga NMR spectra of $Ga(trop)_3$ under 30 kHz MAS at 21.14 T. The simulated spectrum was calculated using the parameters summarized in Table **3.1**. The peaks to either side of the central, high-intensity peak are spinning sidebands. [Page 46]

Figure 3.8 Experimental and calculated ^{71}Ga NMR spectra of stationary $Ga(trop)_3$ at 11.75 and 21.14 T. The simulated spectra were calculated using the parameters summarized in Table **3.1**. [Page 47]

Figure 3.9 Experimental and calculated ^{69}Ga NMR spectra of stationary $Ga(trop)_3$ at 11.75 and 21.14 T. The simulated spectra were calculated using the parameters summarized in Table **3.1**. [Page 48]

Figure 3.10 Experimental and calculated ^{71}Ga NMR spectra of stationary $(NH_4)_3[Ga(cit)_2]\cdot 4H_2O$ at 11.75 and 21.14 T. The simulated spectra were calculated using the parameters summarized in Table **3.1**. [Page 51]

Figure 3.11 Experimental and calculated ^{69}Ga NMR spectra of stationary $(NH_4)_3[Ga(cit)_2]\cdot 4H_2O$ at 21.14 T. The simulated spectra were calculated using the parameters summarized in Table **3.1**. [Page 52]

Figure A2 An example of a good approximation of a skyline projection. Shown is the ^{71}Ga SS NMR spectrum of stationary $(NH_4)_3[Ga(cit)_2]\cdot 4H_2O$ at 11.75 T obtained in 6 windows with WURST-echo pulses in transmitter offset steps of 200 kHz, relative to 0 ppm, from +400 to -600 kHz. All six windows are displayed superimposed (lower trace), and the sum of the six windows is shown (upper trace). [Page 66]

List of Abbreviations and Symbols

Magnetic Shielding and Electric Field Gradient Tensor Parameter Symbols

α, β, γ	Euler angles
C_Q	nuclear quadrupolar coupling constant
ν_Q	quadrupolar frequency
q_{xx}, q_{yy}, q_{zz}	EFG tensor principal components
$\eta_Q,$	quadrupolar asymmetry parameter
δ	chemical shift
δ_{iso}	isotropic chemical shift
$\delta_{11}, \delta_{22}, \delta_{33}$	CS tensor principal components
σ	magnetic shielding
σ_{iso}	isotropic magnetic shielding
$\sigma_{11}, \sigma_{22}, \sigma_{33}$	MS tensor principal components
Ω	powder pattern span (due to CSA / MSA)
κ	powder pattern skew (due to CSA / MSA)

Nuclear Parameter Symbols

γ	magnetogyric ratio
ν_0	Larmor frequency
Ξ	NMR frequency ratio with respect to ^1H
Q	quadrupole moment

Other Symbols

B_0	external magnetic field strength
e	elementary charge

$\hat{H}$	Hamiltonian operator
h	Planck's constant
r	distance between nucleus and surrounding charges (e.g., electrons)
τ	time duration, typically for a pulse or experimental delay parameter
T	Tesla – unit of magnetic field strength

Abbreviations and Acronyms

acac	acetylacetonato ligand
cit	citrato (citrate) ligand
CP	cross-polarization
CS	chemical shift
CSA	chemical shift anisotropy
CT	central transition
CVD	chemical vapour deposition
DFT	density functional theory
EFG	electric field gradient
GIPAW	gauge including projector augmented wave
GTO	Gaussian-type orbital
LED	light emitting diode
MAS	magic angle spinning
MS	magnetic shielding
MSA	magnetic shielding anisotropy
NMR	nuclear magnetic resonance

PAS	principal axis system
PAW	projector augmented wave
QCPMG	quadrupolar Carr-Purcell-Meiboom-Gill pulse sequence
RF	radiofrequency
SS	solid-state
ST	satellite transition
thd	2,2,6,6-tetramethyl-3,5-heptanedionato ligand
TMHD	see thd
WURST	wideband, uniform rate, smooth truncation

Introduction

The element gallium (melting point 29.77 °C, boiling point 2204°C) is a group-13 metal that is present in a very wide variety of useful materials.[1] For example, compounds containing Ga can be found in many semiconductors, solar cell materials, light-emitting diodes (LEDs), and chemical-vapour deposition (CVD) precursors, as well as many medical imaging and anti-cancer agents.[2] However, despite the fact that solid-state (SS) nuclear magnetic resonance (NMR) spectroscopy is a very powerful tool for the spectroscopic characterization of countless solid materials,[3] few Ga-containing compounds have been fully studied by solid-state $^{69/71}$Ga NMR. There are a few notable exceptions, including studies of several gallium oxides,[4] chlorides,[5] MOF-type carboxylates,[6,7] gallium trihalide triarylphosphine complexes,[8] and others,[9] but solid-state $^{69/71}$Ga NMR literature remains relatively sparse. This is quite likely due to the fact that both gallium-69 and gallium-71 nuclei are quadrupolar with spin $I = 3/2$ and with moderately large nuclear quadrupole moments.[10,11] This often leads to very broad powder pattern spectra which may be difficult to acquire. However, recent developments in SS NMR techniques, such as the use of WURST-echo[12] and WURST-QCPMG pulse sequences,[13] together with the availability of ultrahigh-field NMR spectrometers, facilitate the acquisition of extremely broad NMR spectra. Ultrahigh-field NMR spectroscopy can also assist in the differentiation of magnetic shielding anisotropy (MSA) / chemical shift anisotropy (CSA) and electric field gradient (EFG) contributions to the overall NMR powder pattern. This makes it both feasible and

worthwhile to study the $^{69/71}$Ga NMR properties of solid gallium-containing materials.

Since so few materials have been characterized by SS $^{69/71}$Ga NMR, and since so many gallium (III) compounds have important applications, in this investigation we have chosen to study a series of six-coordinate gallium (III) compounds with oxygen coordinated bi- and tridentate ligands.[14] Our goal is to characterize the gallium-69 and -71 NMR parameters in these complexes in order to further our understanding of ^{69}Ga and ^{71}Ga NMR, with the hopes of making ^{69}Ga and ^{71}Ga NMR more accessible as a characterization tool for researchers. Where possible we have selected materials that are commercially available and air-stable, and whose crystal structures have been reported.[2] To begin this study, the well-characterized and relatively simple model β-diketonate tris(acetylacetonato)gallium (III), $Ga(acac)_3$,[15] was examined. This compound has been studied in years past by various current and former members of R.E.W.'s research group, and the unpublished spectra suggested the possible presence of two separate crystallographic Ga sites when only one is expected based on the X-ray diffraction data.[15] In addition, some $^{69/71}$Ga NMR studies for $Ga(acac)_3$ under magic angle spinning (MAS) conditions have been published by a separate research group, and EFG and isotropic chemical shift (but not CSA) parameters have been reported.[16] However, the lack of published CSA parameters for this compound and our curious earlier NMR results motivated us to re-investigate it.

A β-diketonate compound similar to $Ga(acac)_3$, and a chemical vapour deposition (CVD) precursor, tris(2,2,6,6-tetramethyl-3,5-heptanedionato) gallium

(III), $Ga(thd)_3$,[17] was examined by SS $^{69/71}Ga$ NMR. Note that this ligand is sometimes abbreviated (TMHD) rather than (thd) in the literature. The SS NMR properties of tris(tropolonato)gallium (III),[18] $Ga(trop)_3$, were also investigated. Unpubplished preliminary ^{71}Ga and ^{69}Ga studies of $Ga(trop)_3$ have been performed by the Wasylishen group, and this material has radiopharmaceutical applications. The limited available spectra and lack of complementary NMR calculations prompted further investigation. Finally, the tridentate citrate complex of gallium (III), $(NH_4)_3[Ga(C_6H_5O_7)_2]\cdot 4H_2O$,[19,20] hereafter abbreviated $(NH_4)_3[Ga(cit)_2]\cdot 4H_2O$, was investigated too. $[Ga(cit)_2]^{3-}$ is very important in nuclear medicine, and a radiolabelled version of this compound is commonly used in diagnostic gallium scans.[21]

Chapter 1: Background Information and Theory

1.1 The NMR Hamiltonian and the Zeeman Effect

The basics of NMR theory have been well documented.[22-25] While there are many factors that can impact the resonant frequency of a nucleus, in this study we have focused on compounds with single-site gallium nuclei coordinated to oxygen atoms in ligands. Any direct or indirect spin-spin coupling of ^{1}H or other nuclei to gallium was either negligible in our experiments or eliminated with ^{1}H decoupling. As such, the overall NMR Hamiltonian for our ^{69}Ga and ^{71}Ga sites can be represented by:

$$\hat{H} = \hat{H}_Z + \hat{H}_{MS} + \hat{H}_Q \qquad \textbf{(1.1)}$$

where $\hat{H}_Z$, $\hat{H}_{MS}$, and $\hat{H}_Q$ are the Zeeman, magnetic shielding, and quadrupolar contributions to the NMR Hamiltonian, respectively. When placed in a magnetic field, a nucleus, with spin quantum number I, will adopt one of the nuclear magnetic spin states, m_I, with permitted values of $m_I = -I, -I + 1, \ldots, I$. Taking into account only the Zeeman effect, the difference in energy, ΔE, between two neighbouring spin states m_I and $m_I + 1$ corresponds to the Larmor frequency of the nucleus, ν_0, given by:

$$\nu_0 = \frac{\gamma B_0}{2\pi} \qquad \textbf{(1.2)}$$

where B_0 is the strength of the external magnetic field in T and γ is the magnetogyric ratio of the nucleus. Generally, the Larmor frequency falls within the radiofrequency (RF) region of the electromagnetic spectrum. When one considers magnetic shielding, σ, due to the chemical environment at the nucleus, the resonant frequency of the nucleus is slightly modified. In isotropic systems:

$$\nu = \frac{\gamma B_0 (1 - \sigma_{iso})}{2\pi} \quad \textbf{(1.3)}$$

where σ_{iso} is the isotropic magnetic shielding constant.

1.2 Chemical Shift Anisotropy and Tensor Conventions

In NMR spectroscopy, it is standard practice to refer to the effects of magnetic shielding (MS), σ, in terms of chemical shift (CS), δ, rather than magnetic shielding directly. The two properties are related by:[26]

$$\delta = \frac{\nu - \nu_{ref}}{\nu_{ref}} \quad \textbf{(1.4)}$$

$$\delta = \frac{\sigma_{ref} - \sigma}{1 - \sigma_{ref}} \approx \sigma_{ref} - \sigma \quad \textbf{(1.5)}$$

where σ is the absolute magnetic shielding value of the nucleus in question relative to that of a bare nucleus (typically expressed in ppm), σ_{ref} is the absolute magnetic shielding value of the chosen reference compound, δ is the observed chemical shift (typically expressed in ppm) relative to the reference compound, ν is the resonant frequency of the observed nucleus, and ν_{ref} is the resonant frequency of the reference compound. In practice, the chemical shift and magnetic shielding values (in ppm) are independent from external magnetic field strength.

For a given nucleus tumbling about in solution, only the isotropic average of chemical shift / magnetic shielding is observed. However, the chemical shift at a nuclear site in a molecule is actually dependent on the molecule's orientation in an external magnetic field; this is commonly referred to as magnetic shielding

anisotropy (MSA) or chemical shift anisotropy (CSA).[26] A second-rank tensor is used to describe CSA (or MSA). In the orthogonal principal axis system (PAS) of the CS interaction, the symmetric portion of the tensor is diagonal and takes the form:[27,28]

$$\boldsymbol{\delta} = \begin{bmatrix} \delta_{11} & 0 & 0 \\ 0 & \delta_{22} & 0 \\ 0 & 0 & \delta_{33} \end{bmatrix} \quad \textbf{(1.6)}$$

where δ_{11}, δ_{22}, and δ_{33} are known as the principal components of the CS tensor and $\delta_{11} \geq \delta_{22} \geq \delta_{33}$. This method of defining the principal components is known as Mehring notation.[26] When a solid crystalline material is ground into a powder, a distribution of random crystallite orientations will be present. If the NMR spectrum of such a stationary sample is obtained, the result is a so-called "powder pattern". In the absence of any effects other than CSA for a spin I = ½ nucleus, the principal components of the CS tensor correspond to the shoulders and point of discontinuity in the NMR powder pattern (see Figure **1.1**).[29]

Another notation system commonly used when describing the CS tensor principal components is the Maryland convention.[26,30,31] Based on the same principal components used in Mehring notation, this convention defines the CS tensor in terms of the isotropic chemical shift, δ_{iso}, powder pattern span, Ω, and skew, κ:

$$\delta_{\text{iso}} = \frac{1}{3}\left(\delta_{11} + \delta_{22} + \delta_{33}\right) \quad \textbf{(1.7)}$$

$$\Omega = \delta_{11} - \delta_{33} \quad \textbf{(1.8)}$$

$$\kappa = \frac{3\left(\delta_{22} - \delta_{\text{iso}}\right)}{\Omega} \quad \textbf{(1.9)}$$

The Maryland notation is quite convenient for SS NMR spectroscopists because it quickly conveys information on the width of a powder pattern based on Ω, as well as its symmetry and shape, based on κ. Note that Ω is always a positive value expressed in ppm, while κ is unitless and may vary from -1 to +1.[26,31] Figure **1.1** shows some theoretical NMR powder patterns calculated for a spin-1/2 nucleus using Wsolids1[32] with various values of κ, and their corresponding CS tensor principal components in the Mehring convention. Only the CSA interaction is considered in this figure. The principal components δ_{11}, δ_{22}, and δ_{33} have been labelled for each powder pattern as well. Note that the above CS tensor notation conventions correspond to magnetic shielding tensor parameters by the relationship given in Equation **1.5**. That is to say, σ_{11} corresponds to δ_{11}, σ_{22} to δ_{22}, etc., and $\sigma_{11} \leq \sigma_{22} \leq \sigma_{33}$, while Ω and κ follow:

$$\Omega = \sigma_{33} - \sigma_{11} \qquad \textbf{(1.10)}$$

$$\kappa = \frac{3\left(\sigma_{\text{iso}} - \sigma_{22}\right)}{\Omega} \qquad \textbf{(1.11)}$$

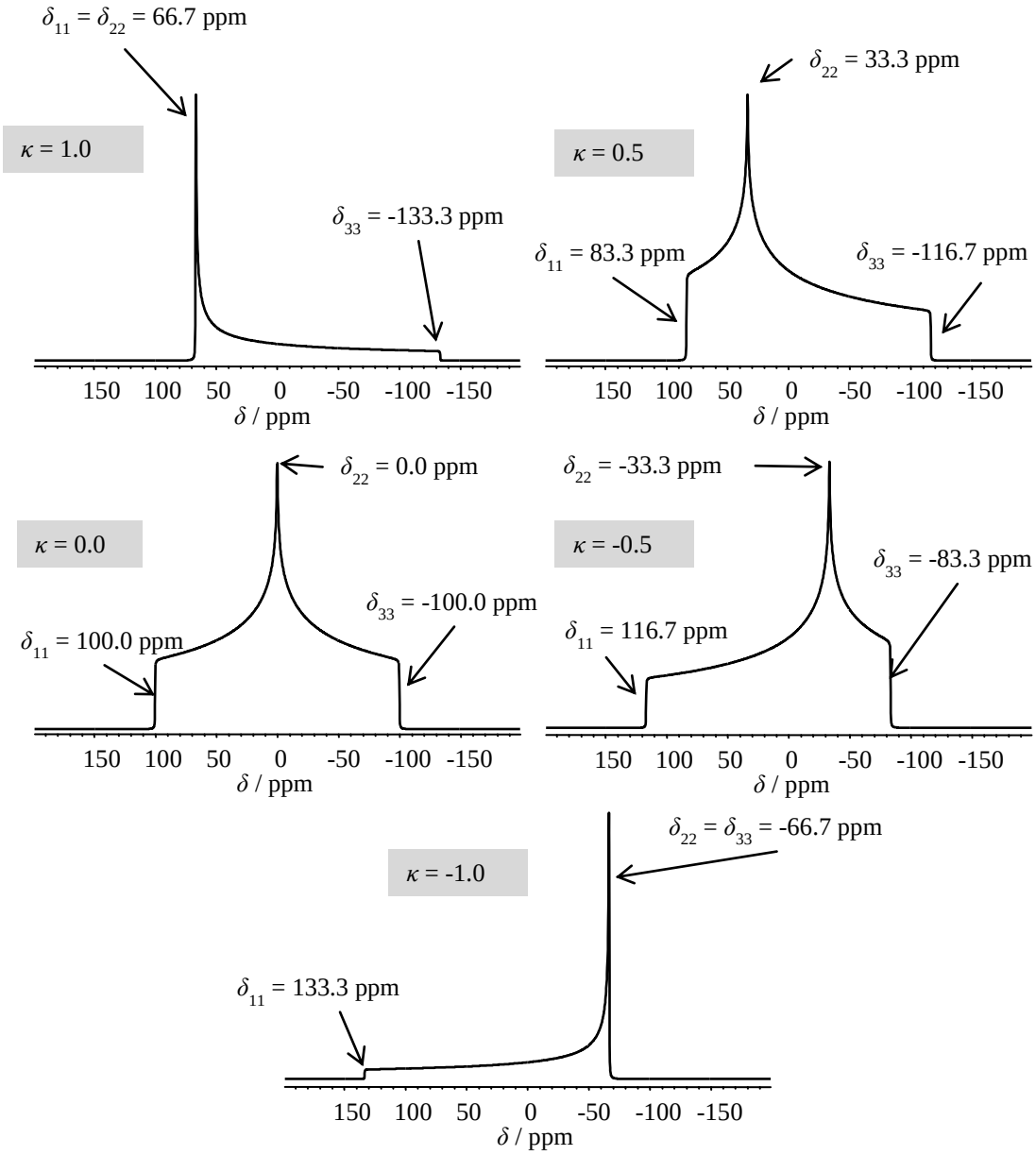

Figure 1.1 Calculated NMR spectra for a spin-1/2 nucleus with $\delta_{iso} = 0$ ppm and $\Omega = 200$ ppm. Different values of κ were used to generate each CSA powder pattern, and the corresponding Mehring notation principal components have been labelled for each spectrum. Spectra were calculated using WSolids1.

1.3 Electric Field Gradients and Quadrupolar Coupling

Thus far, we have discussed the contributions of the Zeeman and magnetic shielding interactions to the overall NMR Hamiltonian. This level of theory is sufficient (in the absence of spin-spin coupling) to characterize the powder patterns of spin-1/2 nuclei. However, nuclei with a spin quantum number $I > ½$ possess a nuclear quadrupole moment, Q. This quadrupole moment can couple with an electric field gradient (EFG) at the nucleus, and quadrupolar coupling[3,29,33-35] gives rise to the $\hat{H}_{\mathrm{Q}}$ contribution of the NMR Hamiltonian.

Like magnetic shielding, the EFG is orientation-dependent and is described by a second-rank tensor. However, the EFG tensor is traceless and symmetric, and has its own orthogonal PAS. It is important to note that the EFG PAS and CSA PAS are not necessarily coincident; that is to say, the relative orientations of the magnetic shielding and quadrupolar interactions may be different. The three diagonal components of the EFG tensor in the PAS, eq_{ii}, are defined such that:[24,29,34]

$$\left|eq_{\mathrm{zz}}\right| \geq \left|eq_{\mathrm{yy}}\right| \geq \left|eq_{\mathrm{xx}}\right| \qquad \textbf{(1.12)}$$

$$eq_{\mathrm{zz}} + eq_{\mathrm{yy}} + eq_{\mathrm{xx}} = 0 \qquad \textbf{(1.13)}$$

The traceless nature of the EFG tensor in the PAS allows it to be characterized with only two parameters. Generally, the EFG at a nucleus is discussed in terms of the quadrupolar coupling constant, C_{Q}, and quadrupolar asymmetry parameter, η_{Q}:[24,29,34]

$$C_{\mathrm{Q}} = \frac{e^2 Q q_{\mathrm{zz}}}{h} \qquad \textbf{(1.14)}$$

$$\eta_{\mathrm{Q}} = \frac{q_{\mathrm{xx}} - q_{\mathrm{yy}}}{q_{\mathrm{zz}}} \qquad \textbf{(1.15)}$$

where e is the elementary charge, Q is the quadrupole moment of the nucleus, and h is Planck's constant. For a given nucleus, C_{Q} is dependent only on the largest component of the EFG tensor, q_{zz}, and is generally expressed in frequency units, while η_{Q} is a unitless quantity ranging in value from 0 to 1.

For half-integer spin quadrupolar nuclei (i.e., those with I = 3/2, 5/2, 7/2, or 9/2), many SS NMR studies focus on the lineshape of the central transition, CT, (m_{I} = +1/2 ↔ -1/2) in the observed NMR powder pattern because this transition is not perturbed, to first order, by the quadrupolar interaction.[29,36] The satellite transitions, STs ($m_{\mathrm{I}} \leftrightarrow m_{\mathrm{I}} - 1$, $m_{\mathrm{I}} \neq ½$), however, are perturbed by the first-order term of the quadrupolar interaction. The full frequency width W due to quadrupolar broadening of a single-quantum NMR transition ($m_{\mathrm{I}} \leftrightarrow m_{\mathrm{I}} - 1$) powder pattern is determined, to first order, by the so-called quadrupolar frequency, ν_{Q}, which is in turn related to C_{Q}:[29,37]

$$\nu_{\mathrm{Q}} = \frac{3C_{\mathrm{Q}}}{2I(2I-1)} \qquad \textbf{(1.16)}$$

$$W = (2m_{\mathrm{I}} - 1)\nu_{\mathrm{Q}} \qquad \textbf{(1.17)}$$

A good approximation of the total width of an NMR powder pattern including all satellite transitions can be obtained by calculating W when $m_{\mathrm{I}} = I$. Equation **1.17** clearly indicates that W = 0 for the CT ($m_{\mathrm{I}} \leftrightarrow m_{\mathrm{I}} - 1$), to first order, since $2m_{\mathrm{I}} - 1 = 0$.

Since the CT is not affected by the quadrupolar interaction to first order, if C_Q is relatively small, the spectrum of the CT is only influenced by the magnetic shielding tensor, and takes on the appearance of a spin-1/2 nucleus powder pattern. However, the CT is perturbed by the quadrupolar interaction to second order, and as such, if C_Q is large enough, its influence dominates the spectrum of the CT. This effect has been described in great detail elsewhere,[38] but a few key points are worth highlighting.

First, the full breadth of the CT powder pattern to second order, $W_{CT}^{(2)}$, is given by:[29]

$$W_{CT}^{(2)} = \frac{\left(\eta_Q^2 + 22\eta_Q + 25\right)}{144\upsilon_0}\left(\frac{9C_Q^2}{\left[(2I)(2I-1)\right]^2}\right)\left(I(I+1) - \frac{3}{4}\right) \qquad \textbf{(1.18)}$$

where η_Q, C_Q, and ν_0 have already been defined. As seen by Equation **1.18**, the quadrupolar contribution to the frequency width of the powder pattern CT depends on C_Q^2 and decreases with increasing field strength since it is inversely proportional to the Larmor frequency. The opposite trend is true for CSA; magnetic shielding causes the CT lineshape to increase in width (in frequency units) with external field. Thus, if one is attempting to differentiate the quadrupolar and CSA contributions to the overall NMR lineshape, acquiring spectra at higher fields can be advantageous since effects due to CSA will be exaggerated with respect to the total lineshape. CSA effects are often dwarfed by the quadrupolar interaction at low field.

Second, while CSA can be completely averaged by techniques such as magic angle spinning (MAS, see Chapter 2.3), the second-order quadrupolar

interaction can only be partially averaged.[39,40] However, under MAS conditions the breadth of the CT powder pattern is reduced and retains a distinctive lineshape. One should note that MAS is usually useful only in cases where it is possible to spin fast enough with respect to CT breadth to avoid the occurrence of spinning sidebands caused by quadrupolar broadening. For CT lineshapes dominated by the quadrupolar interaction, this generally means that ν_{rot} should be at least as fast as one-third of the CT breadth (in frequency units) observed for a stationary sample in order for MAS to be practical. Slower spinning rates may still yield useful spectra, so long as any spinning sidebands do not overlap, or that if they do, the resulting MAS powder pattern may still be reliably simulated. Figure **1.2** shows some calculated CT powder patterns for a ^{71}Ga nucleus at 11.75 T with a C_Q of 4.5 MHz, in the absence of any effects other than quadrupolar coupling, under both stationary and infinitely fast MAS conditions, with different values of η_Q.

Third, as mentioned above, the CSA and EFG tensors each have their own principal axis systems which are not necessarily coincident.[35] Thus, to fully characterize the NMR properties of a quadrupolar nucleus in a solid material, one needs to obtain δ_{iso}, Ω, and κ to define the CS tensor, C_Q and η_Q to define the EFG tensor, as well as three Euler angles,[41] α, β, and γ, to describe the relative orientations of the two tensors' PASs. In this study, the "ZYZ" rotation convention is used, and the EFG PAS is considered the initial frame of reference which is transformed by the Euler angles into the CSA PAS (see references 35, 41, and the Wsolids1[32] user manual). In brief, one can generate the desired axis

system as follows: The two axis systems are initially taken as coincident. Then, the destination frame is rotated about the reference frame's *z*-axis by angle α. Next, the destination frame is rotated about its current intermediate *y*-axis by angle β. Finally, the destination frame is rotated about its *z*-axis by angle γ. Figure **1.3** shows an example of two orthogonal axis systems, X, Y, Z and X', Y', Z', which are related by Euler angles in this manner. Vector coordinates in a reference axis system can be defined with respect to the newly generated axis system via the following transformation matix **T**:[32,41]

$$\mathbf{T} = \begin{bmatrix} \cos\alpha\cos\beta\cos\gamma - \sin\alpha\sin\gamma & \sin\alpha\cos\beta\cos\gamma + \cos\alpha\sin\gamma & -\sin\beta\cos\gamma \\ -\cos\alpha\cos\beta\sin\gamma - \sin\alpha\cos\gamma & -\sin\alpha\cos\beta\sin\gamma + \cos\alpha\cos\gamma & \sin\beta\sin\gamma \\ \cos\alpha\sin\beta & \sin\alpha\sin\beta & \cos\beta \end{bmatrix}$$

1.19

The relative orientation of the two axes can have a profound impact on the CT powder pattern lineshape, but unfortunately they are not easily accessible experimentally. Often, several different combinations of values for α, β, and γ, with no obvious correlation between the sets, can generate visually similar calculated spectra. Computational methods can provide some insight into their values, which assists fitting; however, the results from the computations are of course not definitive. As a result, wide estimated error margins often accompany reported Euler angles.

If the nucleus of interest lies along a crystallographic symmetry element, symmetry places restrictions on the EFG and CSA tensors.[25,33-38,42] For example, if the nucleus lies along a threefold (or greater) axis of rotational symmetry, two CSA principal components must be equivalent, making $\kappa = +1$ (if $\delta_{11} = \delta_{22}$) or $\kappa =$

-1 (if $\delta_{22} = \delta_{33}$), while the third component is oriented parallel to the axis of symmetry, and perpendicular to the plane formed by the two equivalent components. In addition, two of the EFG principal components are equivalent as well, making $\eta_Q = 0$. The largest component of the tensor, q_{zz} is therefore aligned with the axis of symmetry. This in turn restricts the possible values of α, β, and γ. Unfortunately, in this study, no such restrictions exist for the gallium nuclei of interest.

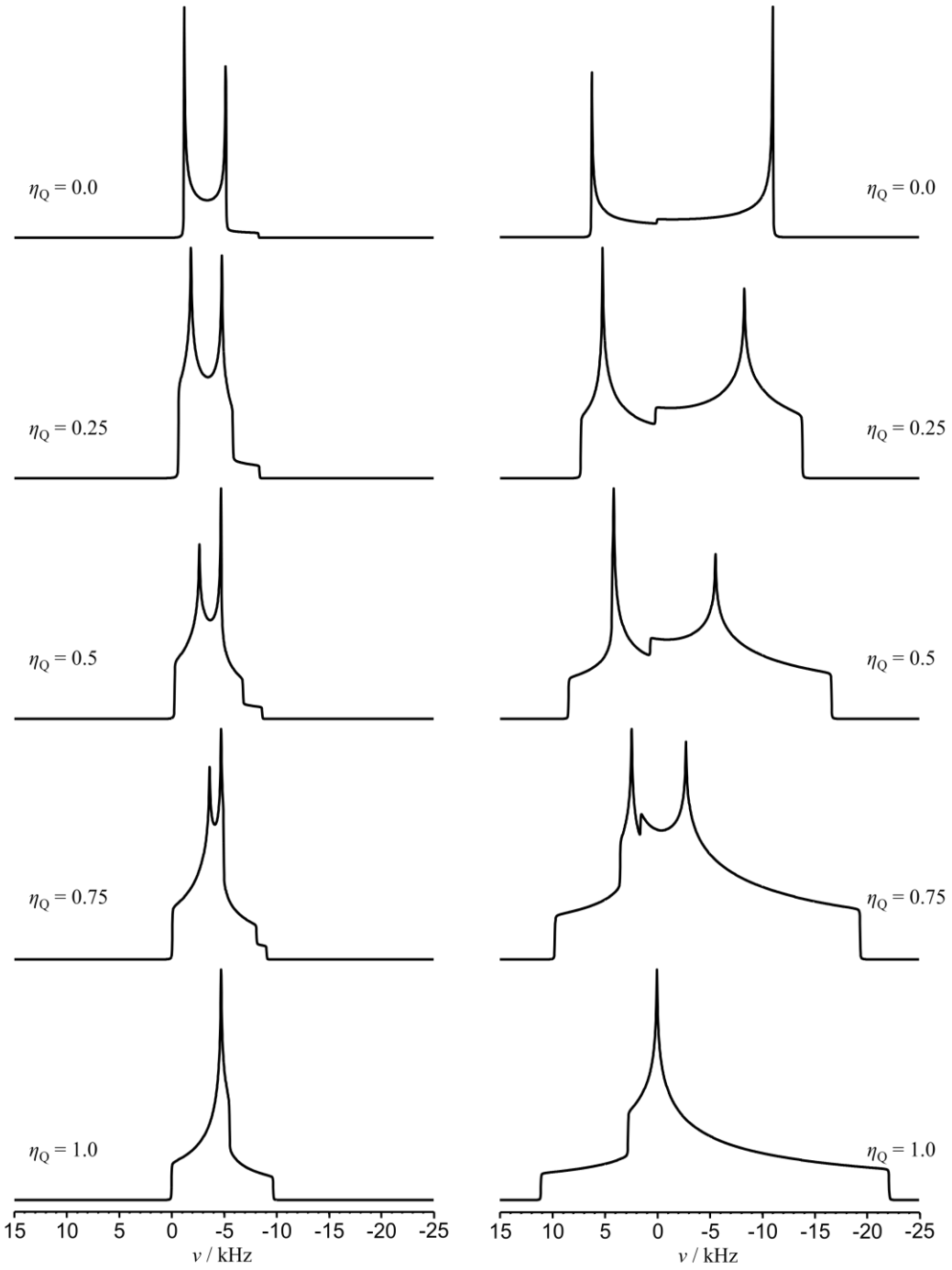

Figure 1.2 Calculated ^{71}Ga NMR spectra at 11.75 T for the central transition of a nucleus with a C_Q = 4.5 MHz and δ_{iso} = 0 ppm, under infinitely fast MAS (left column) and stationary (right column) conditions, with different values of η_Q. CSA effects have been neglected. Spectra were calculated using WSolids1.

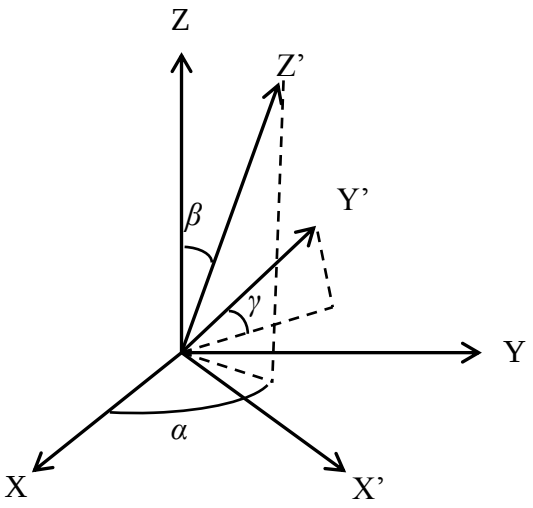

Figure 1.3 Euler angles. The reference axis system is denoted by X, Y, and Z, while the Euler angles α, β, and γ generate the new axis system, X’, Y’, and Z’.

1.4 ^{69}Ga and ^{71}Ga Properties

Both gallium-69 and -71 are spin I = 3/2 nuclei with natural abundances of 60.108 % and 39.892 % respectively.[10,43] ^{69}Ga has a magnetogyric ratio[10] of γ = 6.438 855 x 10^7 rad s^{-1} T^{-1} (frequency ratio Ξ = 24.001 354 % with respect to ^{1}H) and quadrupole moment[11] Q = 17.1 fm^2. For ^{71}Ga, γ = 8.181 171 x 10^7 rad s^{-1} T^{-1} (frequency ratio Ξ = 30.496 704 %) and Q = 10.7 fm^2. Even though ^{69}Ga has a natural abundance greater than ^{71}Ga, ^{71}Ga SS NMR spectra are generally easier to acquire than ^{69}Ga. This is because the larger Q for ^{69}Ga leads to larger quadrupolar coupling constants, and the lower γ for ^{69}Ga causes a lower ν_0 and lower NMR receptivity than ^{71}Ga. By Equation **1.18**, the ^{69}Ga and ^{71}Ga NMR CT powder pattern widths due to the second order term of the quadrupolar interaction are directly proportional to C_Q^2 and inversely proportional to ν_0; for both these reasons, ^{69}Ga CT powder patterns are generally broader than ^{71}Ga CT powder patterns for the same samples. Still, with modern NMR instrumentation and techniques, both ^{69}Ga and ^{71}Ga SS NMR experiments are feasible. This can be particularly advantageous; with two available, naturally occurring nuclei, an NMR spectroscopist can effectively obtain twice as much complementary data with each sample than when conducting NMR experiments on other nuclei.

Chapter 2: Experimental and Computational Methods

2.1 Sample Preparation

Figure **2.1** illustrates the local coordination environment around the gallium centres in each of the four compounds studied. $Ga(acac)_3$ was purchased from Sigma-Aldrich Co. and used without further purification. ^{69}Ga and ^{71}Ga SS NMR spectra were compared to unpublished spectra by Dr. Guy Bernard, a research associate in our lab, as well as published results[16] to confirm the identity of the compound. $Ga(thd)_3$ was purchased from Strem Chemicals Inc. and also used without further purification. Elemental analysis was performed to confirm the identity of the compound, the results of which were (by mass): 64.29 % C (expected 63.98 %) and 9.51 % H (expected 9.27 %).

$(NH_4)_3[Ga(cit)_2]\cdot 4H_2O$ was synthesized according to literature procedures.[19,20] In a typical synthesis, 4.2 mmol of solid $Ga(NO_3)_3\cdot 7H_2O$ and 8.7 mmol of solid citric acid were each dissolved in 20 mL of distilled water and warmed to 40 °C. The solutions were then mixed and stirred while 28-30 % aqueous ammonium hydroxide was added dropwise until the pH of the mixture reached 9. After approximately 6 mL of NH_4OH was added, the final pH was 9.5. The final solution was stirred at 80 °C for approximately 75 minutes. To induce precipitation, some of the solvent needed to be removed with further heating to a final volume of approximately 10 mL. The resulting white precipitate was separated by vacuum filtration, and washed with approximately 5 mL of acetone. The compound was left overnight to dry. The ^{13}C SS NMR spectrum of the compound was acquired, and the results matched those previously reported in the

literature.[19] ^{13}C NMR spectra were acquired at 7.05 T on a Bruker Avance 300 spectrometer under MAS conditions at 10 kHz spinning frequency. The powder sample was packed into a 4 mm thin-walled rotor and a ^{1}H-^{13}C cross-polarization pulse sequence with proton decoupling was used with a ^{1}H 90° excitation pulse length of 4 μs and contact time of 3.0 ms. Spectra were referenced to tetramethylsilane (TMS) by using powdered adamantane as a secondary reference, with the chemical shift of the $^{13}CH_2$ group isotropic peak set to 38.56 ppm.[44] Adamantane was also used as the set-up sample to optimize pulse lengths. The observed ^{13}C SS NMR spectrum matched that in the literature.[19] Carbonyl-region peaks were observed at 190.0, 185.6, 180.9, 179.4, and 173.9 ppm which correspond to the reported values of 189.9, 185.6, 180.7 179.4, and 173.9 ppm within error.

$Ga(trop)_3$ was synthesized according to literature procedures[18] by Ms. Renée Duan, an undergraduate summer student in our lab. The identity of the compound was confirmed via elemental analysis and by comparing obtained $^{69/71}Ga$ NMR spectra to previously unpublished results obtained by Dr. Guy Bernard. The results of the elemental analysis were (by mass): 58.19 % C (expected 58.24 %) and 3.51 % H (expected 3.50 %)

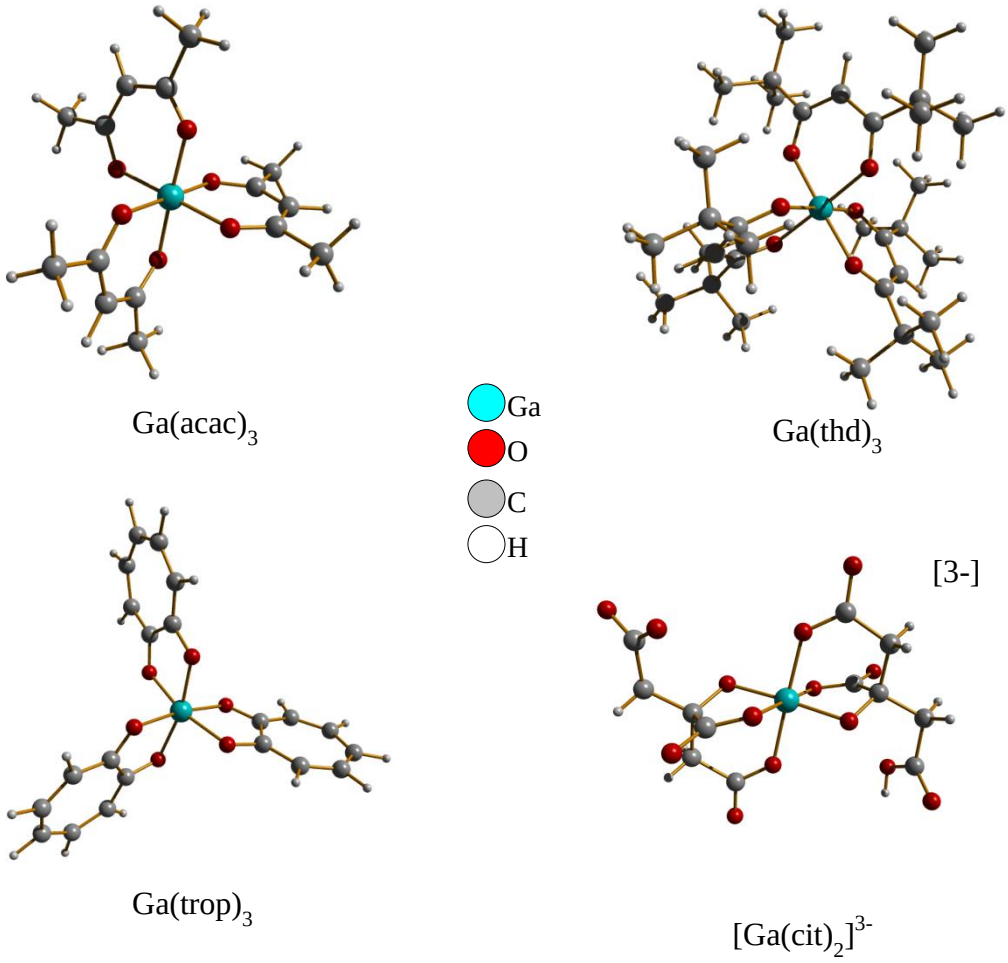

Figure 2.1 Local chemical structure around the gallium centre in each of the four compounds $Ga(acac)_3$, $Ga(thd)_3$, $Ga(trop)_3$, and $(NH_4)_3[Ga(cit)_2]\cdot 4H_2O$. For the citrate complex, only the local $[Ga(cit)_2]^{3-}$ ion is shown. Figures were generated using structure information from the literature.[15,17,18,20]

2.2 $^{69/71}$Ga NMR General Acquisition Techniques

Solid-state ^{69}Ga and ^{71}Ga NMR spectra were acquired at 11.75 T by the author of this thesis on a Bruker Avance 500 spectrometer at the University of Alberta in Edmonton, AB, Canada. Spectra were acquired at 21.14 T on a Bruker Avance II 900 spectrometer at the National Ultrahigh-Field NMR Facility for Solids in Ottawa, ON, Canada by Dr. Victor Terskikh, except for the $Ga(trop)_3$ spectra at 21.14 T, which were acquired by Dr. Shane Pawsey. All spectra were externally referenced[8,10] to 1.0 M (saturated) aqueous $[Ga(H_2O)_6]^{3+}$ from a solution of either gallium nitrate (experiments at Edmonton, AB) or gallium sulfate (experiments at Ottawa, ON), which were also used as setup samples to optimize experimental parameters. Unless otherwise stated, radiofrequency (RF) pulse powers were optimized for simple 4 μs 90° direct excitation pulses on ^{69}Ga or ^{71}Ga. For solid samples a CT selective 90° pulse was used by reducing the pulse length to 2 μs while leaving the pulse power (and therefore excitation nutation frequency) constant. A selective pulse ensures uniform excitation of the CT and is typically useful in cases where C_Q is much larger than the excitation pulse nutation frequency. The pulse duration, τ, of a selective vs. nonselective pulse for a nucleus with spin I is given by:[45,46]

$$\frac{\tau_{\text{nonselective}}}{I+\frac{1}{2}} = \tau_{\text{selective}} \qquad \textbf{(2.1)}$$

Most NMR spectra of stationary powder samples were obtained in single acquisition windows (i.e., the CT powder pattern was narrow enough to fully observe with only one transmitter frequency). Quadrupolar echo $90°_x$-τ-$90°_y$

pulse sequences[47-49] were usually used, with delay time τ ranging from 10-100 μs. Pulse repetition times of 1-2 s were typically employed. ^{1}H decoupling was sometimes used, but seemed to have a negligible effect on any spectra when it was used. Free-induction-decay (FID) acquisition times were on the order of 8-16 ms. Any deviations from these general parameters are noted below.

2.3 Magic Angle Spinning (MAS)

An extremely powerful and frequently-used SS NMR technique is magic angle spinning (MAS).[50,51] In this technique, the powder sample of interest is usually packed into a rotor and floated on a cushion of air while a second stream of air flows across grooves or fins cut into the rotor cap. This causes the rotor to spin rapidly. Narrower rotors are capable of spinning more rapidly, and in this study we used spinning frequencies of up to 25 kHz. Samples for MAS were packed into either 4.0 or 2.5 mm outer diameter rotors depending on the desired spinning rate, while samples for stationary experiments were packed into 5 mm outer diameter glass sample tubes for stationary probes. The angle between the probe RF coil and the external magnetic field was 90° for stationary probes.

In MAS, the probe RF coil and the rotor's axis of rotation is held at an angle of 54°44' relative to the external magnetic field. This is the so-called "magic angle" at which the term $3\cos^2\theta - 1$ equals zero.[22,23] The CSA and dipolar coupling interactions are defined by this mathematical term, and as such, if the sample is spinning at least half as fast as the full frequency width of the CT (i.e., $\nu_{rot} \geq W/2$), their effects on the CT powder pattern are not observed. Only a single

peak at the isotropic chemical shift frequency is then observed in the spectrum (in the absence of quadrupolar interactions). However, if the rotor frequency ν_{rot} is any slower than this, the isotropic peak is observed, as well as spinning sideband peaks spaced about it, separated from the isotropic peak and one another by the same frequency as ν_{rot}. These spinning sidebands will generally follow the shape and width of the CT powder pattern, with each peak representing a weighted average of a portion of the powder pattern. Not only does this technique have the advantage of isolating the isotropic chemical shift, but it effectively compresses the signal from an entire powder pattern into a single peak (or series of peaks), which can greatly increase the spectrum's signal-to-noise ratio (S/N). Note that the isotropic peak position is independent from the rotor frequency (in the absence of sample heating due to MAS), and it can be advantageous to obtain spectra with different spinning rates to unambiguously determine the true isotropic chemical shift.

As mentioned in Chapter 1, MAS does not completely eliminate the second-order effects of the quadrupolar interaction on an NMR spectrum (see Figure **1.2**).[35] Nonetheless, if the sample undergoes sufficiently fast MAS, the observed CT powder pattern is narrowed and dependent only on δ_{iso}, C_Q, and η_Q. This greatly simplifies the determination of several CSA and EFG tensor principal components. It is important to note that when using echo-type pulse sequences, the pulses must be rotor-synchronized; that is to say, the length of time between the center of each excitation pulse must be a multiple of the spinning period, $1/\nu_{rot}$. It should also be noted that, as can be seen in Figure **1.2**, the centre of mass

of the CT MAS powder pattern often does not coincide with the isotropic shift. This phenomenon is referred to as the second-order quadrupolar shift.[42]

2.4 Broad Powder Patterns and WURST Pulses

As previously mentioned, in this study the standard quadrupolar echo $90°_x$-τ-$90°_y$ pulse sequence was most often used, but sometimes the observed CT powder pattern was too broad to fully excite and observe with a single transmitter frequency. In these cases, it was necessary to acquire a series of spectral windows at different transmitter frequencies and "stitch" the resulting spectra together by plotting only data points from individual spectra with the highest signal intensity at a given frequency point. This is commonly referred to as a "skyline projection".[52-54] Alternatively, if enough individual spectral windows are obtained with narrow transmitter offset separations, a suitably distortion-free spectrum can be obtained by simply plotting the sum of the spectral windows. In this study, spectra composed of multiple acquisition windows are compiled in this manner. As an example, Figure **A2** in Appendix 2 shows how the ^{71}Ga SS NMR spectrum for stationary $(NH_4)_3[Ga(cit)_2]\cdot 4H_2O$ at 11.75 T was obtained from a summation of six different acquisition windows.

Sometimes, however, the CT powder pattern obtained was extremely broad, and would have required too many quadrupolar echo windows to acquire in a reasonable amount of time. In such cases, wideband, uniform rate, smooth truncation (WURST) pulses were used in place of standard pulses for WURST-echo experiments.[12,13,55,56] These adiabatic pulses are generally long (we used

pulse lengths of 50 μs) and allow for uniform excitation across a broad range of frequencies (our pulses were 1 MHz wide). When used, excitation frequency is swept across the WURST pulse region over its duration. We tried acquiring WURST-echo spectra sweeping from both high-to-low and low-to-high frequencies with no observable difference in the resulting powder patterns.

Due to probe limitations, it was still necessary to acquire several spectral windows with WURST pulses; however, fewer windows were required than if standard rectangular pulses were employed. Generally, spectral windows acquired with WURST pulses suffer a loss in S/N compared to those acquired using standard hard pulses with the same number of acquisitions, but the fewer number of windows required leads to an overall reduction in experiment time to obtain a skyline projection with comparable S/N.[12,13]

2.5 Summary of NMR Experiments

The ^{71}Ga SS NMR spectrum acquired for $(NH_4)_3[Ga(cit)_2]\cdot 4H_2O$ at 11.75 T was obtained in 6 windows with WURST-echo pulses in transmitter offset steps of 200 kHz, relative to 0 ppm, from +400 to -600 kHz. WURST-QCPMG[13] experiments were attempted for this compound, but no signal was observed, likely due to short T_2 (spin-spin relaxation) times for the gallium nucleus. The ^{69}Ga NMR spectrum of $Ga(trop)_3$ at 11.75 T was also acquired using a WURST-echo pulse, in a single acquisition window. All other ^{71}Ga and ^{69}Ga spectra at all fields were acquired using $90°_x$-τ-$90°_y$ pulse sequences, except for the ^{71}Ga NMR spectrum of $Ga(trop)_3$ at 21.14 T under MAS, in which a $90°_x$-

τ-180°$_y$ pulse sequence was used. For MAS samples, non-selective (4 μs) pulses were used, and for stationary samples, selective (2 μs, unless otherwise stated) pulses, except for the ^{71}Ga NMR spectrum of Ga(thd)$_3$ at 11.75 T under MAS, in which selective pulses were used. The ^{71}Ga SS NMR spectrum for $(NH_4)_3[Ga(cit)_2]\cdot 4H_2O$ at 21.14 T was obtained in two acquisition windows with transmitter offsets of +200 and -300 kHz relative to 0 ppm to ensure no spectral distortions were present due to probe limitations. The ^{69}Ga SS NMR spectrum for the same compound at 21.14 T is the result of 11 spectral windows at 200 kHz transmitter offset intervals ranging from +750 to -1250 kHz relative to 0 ppm. Also at 21.14 T, the ^{69}Ga SS NMR spectrum of Ga(thd)$_3$ was acquired in three windows at transmitter offset separations of 50 kHz, with selective pulse lengths of 1.5 μs. All other spectra were acquired using a single transmitter offset.

2.6 Calculation of Theoretical Spectra

To analyze the obtained spectra and extract the NMR parameters of interest, experimental spectra were compared to simulated spectra calculated using the program Wsolids1[32] ver. 1.20.15 (2011). Wsolids was developed by several members of Dr. R. Wasylishen's research group at Dalhousie University in the late 1980s and 1990s. The current version of the program, Wsolids1, is developed and maintained by Dr. K. Eichele at the Universität Tübingen. It permits the calculation of NMR spectral lineshapes for nuclei under both MAS and stationary conditions, calculating CT and/or ST powder patterns. Among other things, it accounts for the CSA and quadrupolar interactions up to the

second-order level of theory, which we found sufficient for our studies, as well as the relative orientations of the CSA and EFG tensors. All calculated spectra in this study were generated using Wsolids1, and various NMR parameter sets were attempted until visually acceptable fits of the experimental data were obtained. Errors in reported NMR parameters were estimated based on the range of parameter values that generated largely indistinguishable spectra, as well as any discrepancies between parameters obtained for data at different field strengths.

2.7 Computational Methods

To assist in the determination of ^{69}Ga and ^{71}Ga NMR parameters, calculations on the four compounds studied herein were performed from first principles methods using CASTEP.[57] The program was used to calculate NMR shielding[58,59] and EFG tensors.[60] Calculations were performed by Dr. Victor Terskikh at the National Ultrahigh-Field NMR Facility for Solids in Ottawa, ON, Canada. Most calculations took less than one week of computational time, but the calculation on $(NH_4)_3[Ga(cit)_2]\cdot 4H_2O$ took 8 days. Calculation results from CASTEP output files were summarized using EFGShield ver. 3, a program developed in Dr. David Bryce's lab at the University of Ottawa in Ottawa, ON, Canada.[61,62] EFGShield parses the output files of some computational chemistry programs that calculate EFG and shielding tensor parameters and extracts the tensors' principal components and Euler angles.

CASTEP makes use of the Gauge Including Projector Augmented Wave (GIPAW) and Projector Augmented Wave (PAW) approaches to calculating

shielding and EFG parameters. The theory and methods behind these computational techniques are well discussed elsewhere,[63,64] but will be very briefly summarized here. These techniques rely on Density Functional Theory (DFT) and make use of periodic planewave basis functions rather than basis functions such as Gaussian-type orbitals (GTO) as in traditional Hartree-Fock methods.[63] Often core electrons are held frozen, and pseudopotentials are used to describe the interactions between core and valence electrons.[64] Overall, the PAW and GIPAW can be much more efficient at calculating EFG and magnetic shielding tensor parameters for periodic solid systems than Hartree-Fock type calculations on large clusters of atoms.[63,64]

A summary of all calculation results is presented in Table **3.2**. Calculations were performed on $Ga(acac)_3$ using the reported crystal structure.[15] It was necessary to add hydrogen atoms to the crystal structure, as they were not included in the reported structure. C-H bond lengths of 1.089 Å were used. Due to size constraints, the symmetry of the system was reduced to primitive, and two molecules were isolated rather than using a full unit cell. The "medium" basis set accuracy setting was used. NMR parameter calculations were performed before and after a geometry optimization; the results of the NMR calculations after geometry optimization have been reported in Table **3.2**, as they appeared to slightly more closely match the experimental results.

Since the only structural information available for $Ga(thd)_3$ was a molecular structure obtained from computational methods,[17] the CASTEP calculation was performed on a single molecule. As such, the results are less than

reliable. The "medium" basis set accuracy setting was used for this calculation. Calculations on $Ga(trop)_3$ were performed with a full unit cell, but under the "coarse" accuracy setting, using reported structural parameters.[18] It was noted by Dr. Terskikh that in the reported crystal structure, two of the hydrogen atoms, H7 and H7B were actually oriented in the wrong direction; this was corrected before CASTEP calculations were performed.

The literature $(NH_4)_3[Ga(cit)_2]\cdot 4H_2O$ structure[20] contained the largest unit cell, and as such it was necessary to reduce the structure to two $[Ga(cit)_2]^{3-}$ ions, counterbalanced with the appropriate number of ammonium ions and water molecules as demanded by the stoichiometry. The "medium" accuracy setting was employed.

Chapter 3: Results and Discussion

3.1 Results Overview

Figures **3.1** through **3.11** show the ^{69}Ga and ^{71}Ga spectra obtained for $Ga(acac)_3$, $Ga(thd)_3$, $Ga(trop)_3$, and $(NH_4)_3[Ga(cit)_2]\cdot 4H_2O$ at 11.75 and 21.14 T under stationary and MAS conditions. All spectra, experimental and calculated, show only the central ^{69}Ga or ^{71}Ga transition, excluding all of the satellite transitions.

Simulated spectra calculated using Wsolids1[32] are shown along with the experimental spectra. For stationary samples, simulations calculated taking into account only the quadrupolar interaction ("EFG only"), only the magnetic shielding interaction ("CSA only"), and the combined effects of both interactions ("EFG + CSA") are shown to highlight the extent to which each interaction influences the overall powder pattern. The NMR parameters extracted from this fitting procedure are summarized in Table **3.1**, along with their estimated errors. The results of CASTEP calculations are summarized in Table **3.2**. Note that CASTEP calculates the principal components (eq_{ii}) of the EFG tensor; we have used these components along with Equation **1.14** and the values of Q for ^{69}Ga and ^{71}Ga listed in Chapter 1.4 to calculate the C_Q values reported in Table **3.2**.

Table 3.1 Summary of experimental ^{69}Ga and ^{71}Ga NMR parameters for $Ga(acac)_3$, $Ga(thd)_3$, $Ga(trop)_3$, and $(NH_4)_3[Ga(cit)_2]\cdot 4H_2O$. Some equivalent Euler angle values that generated visually identical calculated spectra are given in parenthesis.

	$Ga(acac)_3$	$Ga(thd)_3$	$Ga(trop)_3$	$(NH_4)_3[Ga(cit)_2]\cdot 4H_2O$
$\lvert C_Q(^{69}Ga)\rvert$ / MHz	10.58 ± 0.04	10.4 ± 0.1	17.4 ± 0.2	-45.0 ± 0.5[b]
$\lvert C_Q(^{71}Ga)\rvert$ / MHz	6.62 ± 0.04	6.50 ± 0.05	10.98 ± 0.05	-28.4 ± 0.5[b]
η_Q	0.16 ± 0.01	0.40 ± 0.02	0.10 ± 0.01	0.48 ± 0.01
δ_{iso} / ppm	-10.4 ± 0.1	-5.5 ± 0.5	106.0 ± 0.3	52 ± 5
Ω / ppm	< 20[a]	60 ± 15	45 ± 10	260 ± 15
κ	≈ 0.7[a]	0.54 ± 0.20	-0.3 ± 0.2	0.35 ± 0.10
α / °	≈ 64[a]	114 ± 20	0 ± 10	17 ± 5 (197 ± 5)
β / °	≈ 82[a]	70 ± 20	90 ± 5	0 ± 2
γ / °	≈ 4[a]	120 ± 20	0 ± 20	82 ± 2 (262 ± 2)

[a] Values are approximate estimations, as a conclusive fit could not be obtained. See text.
[b] $\lvert C_Q(^{69}Ga)\rvert$ = 45.0 ± 0.5 MHz and $\lvert C_Q(^{71}Ga)\rvert$ = 28.4 ± 0.5 MHz, however, we are confident that the sign of the quadrupolar coupling constants are negative. See text.

Table 3.2 Summary of CASTEP calculated ^{69}Ga and ^{71}Ga NMR properties for $Ga(acac)_3$, $Ga(thd)_3$, $Ga(trop)_3$, and $(NH_4)_3[Ga(cit)_2]\cdot 4H_2O$.

	$Ga(acac)_3$[b]	$Ga(thd)_3$[c]	$Ga(trop)_3$	$(NH_4)_3[Ga(cit)_2]\cdot 4H_2O$
$C_Q(^{69}Ga)$ / MHz	8.844	9.632	14.355	-35.397
$C_Q(^{71}Ga)$ / MHz	5.534	6.027	8.982	-22.149
η_Q	0.142	0.009	0.096	0.488
σ_{iso} / ppm	1725	1708	1581	1624
δ_{iso} / ppm[a]	89	106	233	190
Ω / ppm	20.3	11.6	33.1	279.1
κ	-0.26	-0.97	0.12	0.26
α / °	244	6	180	199
β / °	82	87	90	-3
γ / °	147	180	0	262
Structure Reference	15	17	18	20

[a] Calculated isotropic shielding parameters were converted to chemical shifts based on the previously calculated[8] absolute shielding value of σ_{iso} = 1814 ppm for the reference compound, 1.0 M aqueous $[Ga(H_2O)_6]^{3+}$, whose isotropic shift δ_{iso} = 0.0 ppm.
[b] Results after addition of H atoms and geometry optimization
[c] Calculation performed on a single molecular structure obtained computationally, as crystal structure data was not available.

3.2 $Ga(acac)_3$

When the $Ga(acac)_3$ sample was first obtained from the Sigma Aldrich Co., a ^{71}Ga NMR spectrum of the stationary powder was obtained at 11.75 T. Curiously, the spectrum took the appearance of two overlapping quadrupolar powder patterns with very similar chemical shifts but slightly different EFG parameters. This suggested that two crystallographic Ga sites were present in the sample in approximately equal proportions when only one was expected based on the reported crystal structure.[15] It was plausible that the sample contained two or more polymorphs of $Ga(acac)_3$. Dimorphism for $Ga(acac)_3$ has been previously suggested by Jaeger in 1930;[65] while it primarily crystallizes in a monoclinic system, an orthorhombic form may exist, too. The monoclinic form dominates when $Ga(acac)_3$ is recrystallized from methanol, and crystals grown from this solvent were used in the X-ray diffraction study that solved its structure. [15] So, to isolate the monoclinic form of $Ga(acac)_3$, approximately 0.5 g of the solid was dissolved in about 20 mL of methanol and left to stand overnight. By the next day, the solvent had evaporated, and the resulting crystals were very gently ground using a mortar and pestle before being packed into a rotor or sample tube. The ^{71}Ga NMR spectrum of stationary recrystallized $Ga(acac)_3$ was obtained at 11.75 T, and the resulting spectrum appeared to contain signal from only one unique gallium site. Only $Ga(acac)_3$ recrystallized from methanol was used in all subsequent experiments.

Figure **3.1** shows the ^{71}Ga NMR spectrum of $Ga(acac)_3$ with 10 kHz MAS obtained at 21.14 T. The quadrupolar MAS powder pattern is shown in the centre

of the spectrum, and the low-intensity lineshapes to either side of the main signal are the result of spinning sidebands. A theoretical spectrum was calculated using Wsolids1 and visually fit to the experimental spectrum. From this we were able to extract the parameters δ_{iso} = -10.4 ± 0.1 ppm, $|C_Q(^{71}Ga)|$ = 6.62 ± 0.04 MHz, and η_Q = 0.16 ± 0.01. These agree reasonably well with the parameters reported by Chae *et al.*[16] of δ_{iso} = -10.5 ± 0.5 ppm, $|C_Q(^{71}Ga)|$ = 5.9 MHz, and η_Q = 0.12. Note that the authors of this paper did not recrystallize their sample, and this may account for the slight discrepancy between their values and ours. The value for $|C_Q(^{71}Ga)|$ also agrees well with that reported by Dechter et. al.[66] of 6.6 MHz, which was obtained from solution NMR studies. Our obtained value for the magnitude of $C_Q(^{71}Ga)$ also agrees reasonably well with the results of the CASTEP calculations (within approximately 20 %) in Table **3.2**, as does the value for η_Q.

In order to elucidate the CSA tensor parameters for $Ga(acac)_3$, ^{71}Ga and ^{69}Ga NMR spectra were acquired for stationary samples at 11.75 T and 21.14 T, as seen in Figures **3.2** and **3.3** respectively. It quickly became apparent that while effects due to magnetic shielding definitely have some effect on the overall powder pattern, this effect is fairly minor in comparison to that of the quadrupolar interaction. As expected, the ^{71}Ga NMR spectrum at 21.14 T (Figure **3.2**) is most influenced by CSA. Compared to the "EFG only" simulation, the "CSA + EFG" simulation powder pattern's low- and high-frequency horns are shifted slightly towards the centre of the spectrum, and two shoulders rather than one are observable at the low-frequency end of the powder pattern. This is reflected in

the experimental spectrum. This migration of quadrupolar powder pattern horns when CSA is taken into account is not strongly evident in the other ^{71}Ga and ^{69}Ga NMR spectra, and only a hint of the second low-frequency shoulder is observable in the ^{71}Ga spectrum at 11.75 T and ^{69}Ga spectrum at 21.14 T.

The spectra were fit using Wsolids1. The parameters obtained from MAS experiments (δ_{iso}, C_Q, and η_Q) were used in the calculated spectra for stationary samples. $|C_Q(^{69}Ga)|$ was determined from $|C_Q(^{71}Ga)|$ based on the ratio of the two nuclei's quadrupole moments.[11] As follows from Equation **1.14**, for two nuclei in the same environment, $[C_Q(^{69}Ga)] = [C_Q(^{71}Ga)][Q(^{69}Ga)/Q(^{71}Ga)]$, where Q for the two nuclei are given in Chapter 1.4. In principle, $|C_Q(^{69}Ga)|$ can be exactly determined this way. However, the ^{71}Ga NMR spectrum fit was imperfect (hence the error in $|C_Q(^{71}Ga)|$), so $|C_Q(^{69}Ga)|$ needed to be slightly adjusted until an acceptable fit of the stationary sample spectra was obtained. This discrepancy was considered when determining an estimate of error in $|C_Q(^{69}Ga)|$ and $|C_Q(^{71}Ga)|$. Keeping in mind some preliminary values obtained from the CASTEP calculations, various values for the gallium CSA parameters were used when fitting the spectra. Unfortunately, since the magnetic shielding interaction has such a minor influence on the NMR spectra at the fields studied, conclusive CSA tensor parameters could not be obtained. However, we can say with confidence that the span Ω is likely less than 20 ppm, with an approximate value of 17 ppm, while approximate values of κ and the Euler angles are summarized in Table **3.1**. The spectra calculated using these parameters are shown with the experimental spectra in Figures **3.2** and **3.3**. The fits are imperfect; one can note the slight

mismatch between calculated and experimental spectra for the high-frequency powder pattern horn in the ^{71}Ga NMR spectrum at 21.14 T. Also, it appears that there may be some splitting in the low-frequency horn of the ^{69}Ga NMR spectrum at 21.14 T that is not reproduced in the calculated spectrum. Nonetheless, the calculated powder patterns reproduce the experimental spectra reasonably well.

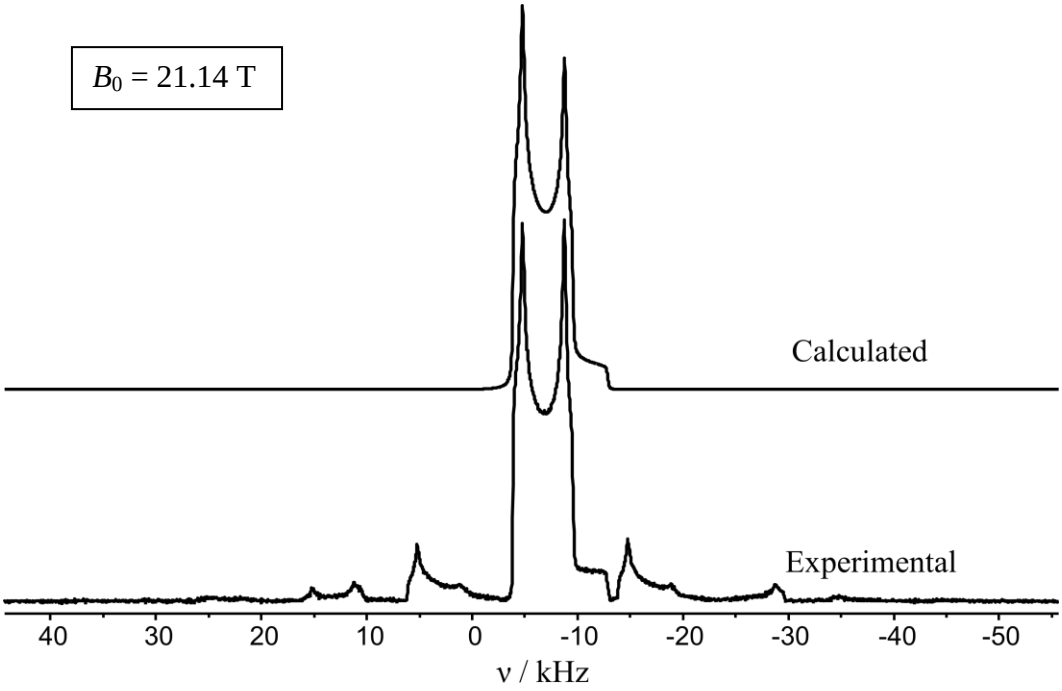

Figure 3.1 Experimental and calculated ^{71}Ga NMR spectra of $Ga(acac)_3$ under 10 kHz MAS at 21.14 T. The simulated spectrum was calculated using the parameters summarized in Table **3.1**. The peaks to either side of the central, high-intensity peak are spinning sidebands.

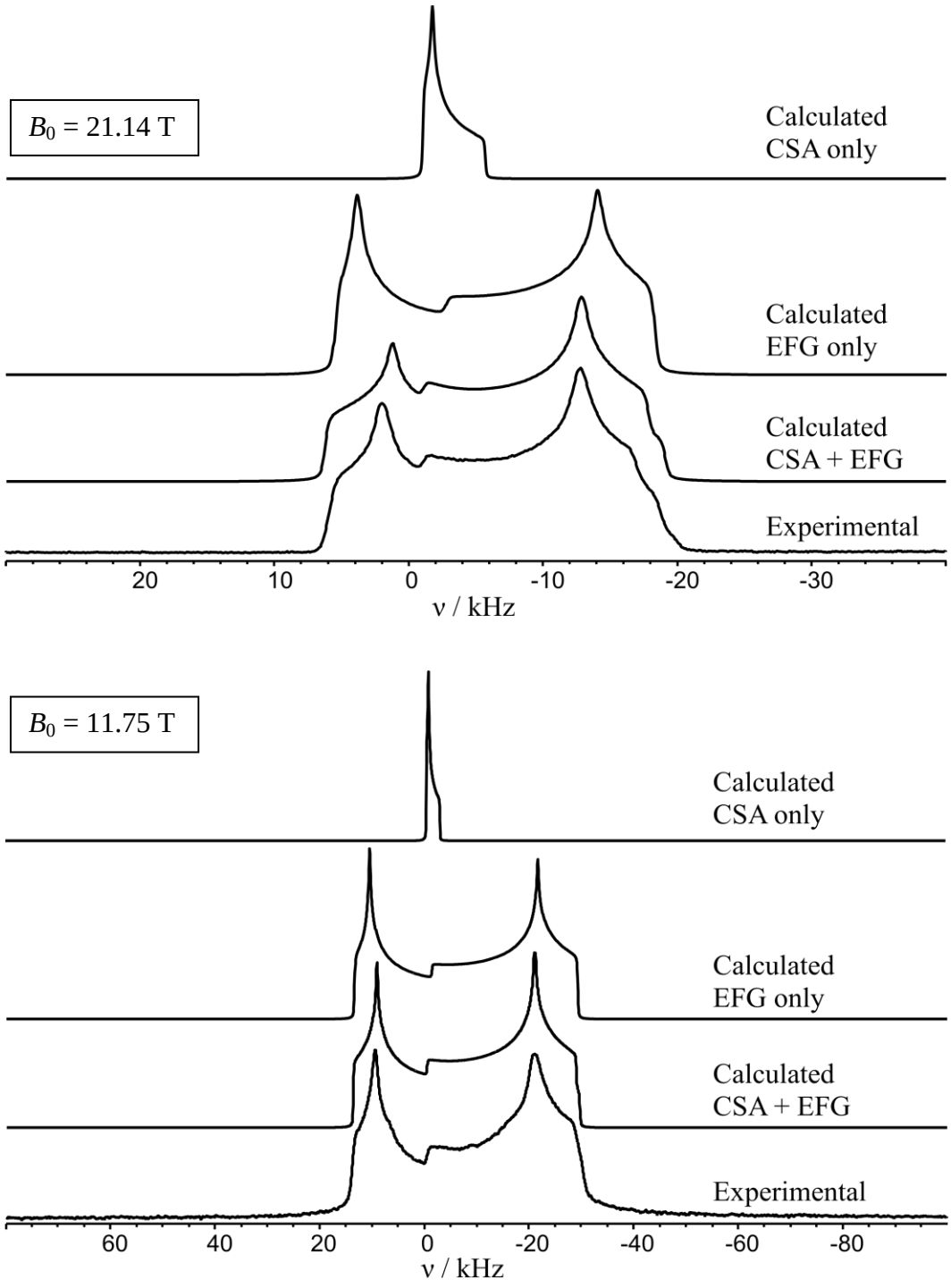

Figure 3.2 Experimental and calculated ^{71}Ga NMR spectra of stationary $Ga(acac)_3$ at 11.75 and 21.14 T. The simulated spectra were calculated using the parameters summarized in Table **3.1**, but with Ω = 17 ppm (see text).

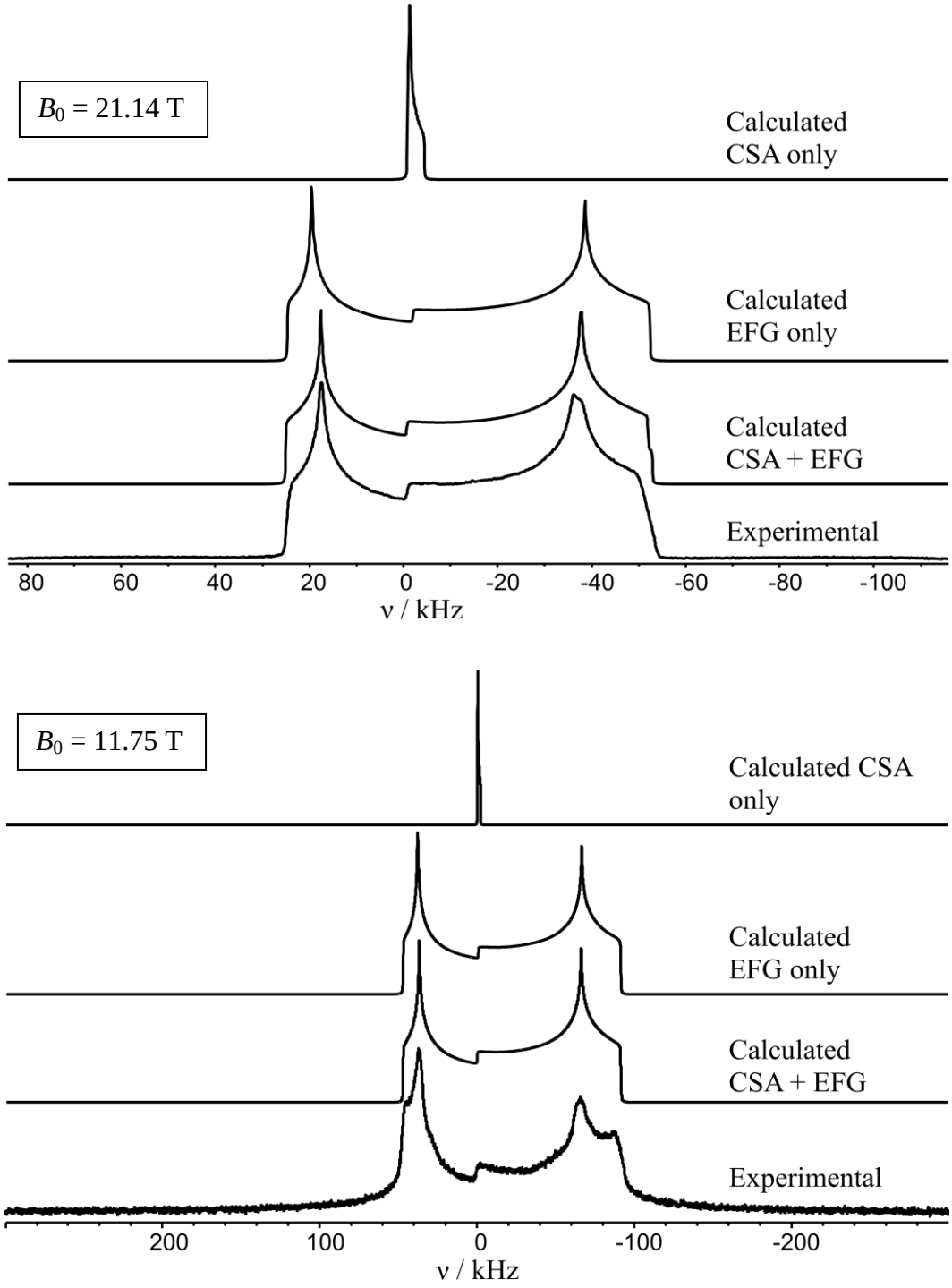

Figure 3.3 Experimental and calculated ^{69}Ga NMR spectra of stationary $Ga(acac)_3$ at 11.75 and 21.14 T. The simulated spectra were calculated using the parameters summarized in Table **3.1**, but with Ω = 17 ppm (see text).

3.3 Ga(thd)$_3$

^{71}Ga NMR spectra of Ga(thd)$_3$ under MAS at 11.75 and 21.14 T are shown in Figure **3.4**. Using the same fitting procedure as for Ga(acac)$_3$, the parameters $|C_Q(^{71}Ga)|$ = 6.50 ± 0.05 MHz, η_Q = 0.40 ± 0.02, and δ_{iso} = -5.5 ± 0.5 ppm were obtained; calculated spectra are shown along with the experimental results. A slight discrepancy in C_Q and δ_{iso} between the spectra obtained at the two fields was the basis for our estimate of error margins for these values, and all other errors were estimated using methods previously described. As with Ga(acac)$_3$, $|C_Q(^{69}Ga)|$ was obtained from $|C_Q(^{71}Ga)|$ based on the ratio of the two nuclei's quadrupole moments, then adjusted slightly until an acceptable fit of the stationary sample spectra was obtained.

^{71}Ga and ^{69}Ga NMR spectra of stationary samples of Ga(thd)$_3$ are shown in Figures **3.5** and **3.6** respectively. The CSA parameters and Euler angles for this compound proved especially difficult to fit. Unfortunately, a crystal structure for this compound has not been reported, and only a molecular structure obtained from computational methods[17] is available in the literature. As such, CASTEP calculations were performed on an isolated molecule rather than a true periodic system (summarized in Table **3.2**). While the calculated value for $C_Q(^{71}Ga)$ of 6.027 MHz is sensible, being within 10 % of the experimentally determined value, all other calculated parameters proved to be of little use in fitting the stationary ^{71}Ga and ^{69}Ga NMR spectra of Ga(thd)$_3$. Theoretical spectra calculated using parameters obtained from CASTEP calculations bore little resemblance to the experimental spectra. To fit the stationary spectra, it was necessary to

determine five separate parameters (Ω, κ, α, β, γ) manually, with no good initial estimate as to their values (values for C_Q, η_Q, and δ_{iso} were already obtained from experiments on samples under MAS). It should be noted that these parameters are not independent with regards to their effects on the calculated spectra. That is to say, no one parameter is responsible for a specific feature of the CT lineshape. They are all related, and all affect the entire powder pattern. Nonetheless, through trial-and-error, various parameter sets were attempted until a visually acceptable fit of CSA tensor components and Euler angles was obtained, summarized in Table **3.1**. The fit is not ideal, as there is a good deal of mismatch between calculated and experimental spectra at both fields, for both nuclei, and as such the estimated error margins for these parameters are quite wide. Further refinement of the parameters through trial-and-error might improve the quality of the fit, but without further information or alternative fitting techniques, this is unlikely. More accurate CASTEP calculations could yield better parameters if the crystal structure of the material is solved. However, under the circumstances and given the variability of the parameters involved in the fitting procedure, the calculated lineshapes are in reasonably good agreement with the experimental spectra.

$Ga(thd)_3$ is similar to $Ga(acac)_3$ in chemical composition and local Ga coordination, so it is not surprising that the two have very similar quadrupolar coupling constants (see Table **3.1**). What is surprising, however, is that the two materials exhibit very different CSA properties at the Ga site; the span Ω of 60 ± 15 ppm for $Ga(thd)_3$ is approximately 3 times that for $Ga(acac)_3$. This suggests that the local [GaO_6] octahedra in solid $Ga(thd)_3$ probably deviate more from

octahedral symmetry than they do in $Ga(acac)_3$. Nuclei in environments of perfect tetrahedral, octahedral, or cubic long-range symmetry will have a C_Q and Ω of zero.[42] Especially for the ^{71}Ga NMR spectrum of a stationary sample acquired at 21.14 T (Figure **3.5**), effects of CSA on the overall CT lineshape are quite dramatic. The breadth of the "CSA only" simulation is nearly as large as that of the "EFG only" spectrum, clearly showing that both play a major role in defining the overall lineshape.

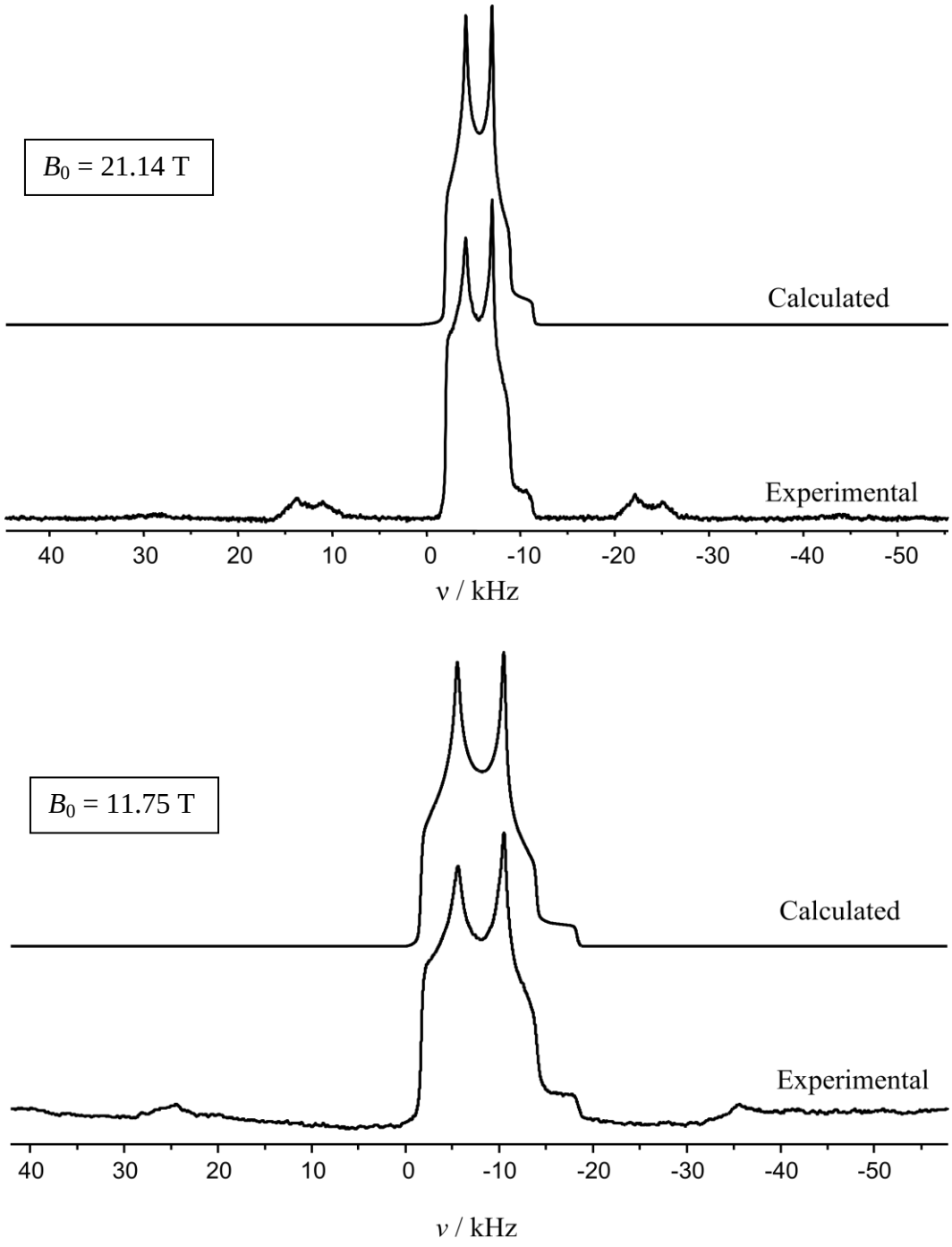

Figure 3.4 Experimental and calculated ^{71}Ga NMR spectra of Ga(thd)$_3$ under 18 kHz MAS at 21.14 T and 30 kHz MAS at 11.75 T. The simulated spectrum at 21.14 T was calculated using the parameters summarized in Table **3.1**, while the one at 11.75 T was calculated using C_Q = 6.47 MHz, η_Q = 0.40, and δ_{iso} = -5.0 ppm (these agree within error). The peaks to either side of the central, high-intensity peak in each spectrum are spinning sidebands.

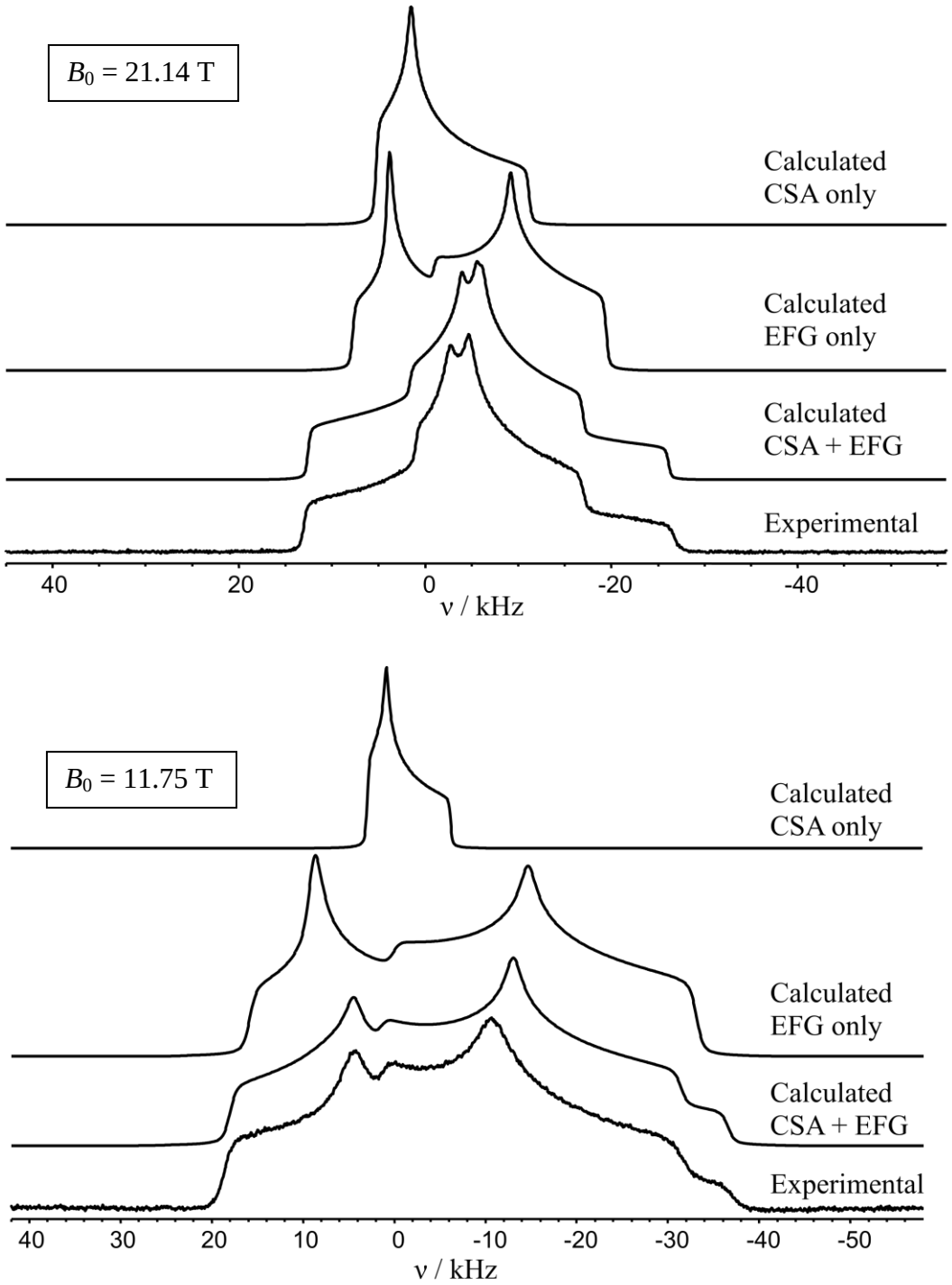

Figure 3.5 Experimental and calculated ^{71}Ga NMR spectra of stationary $Ga(thd)_3$ at 11.75 and 21.14 T. The simulated spectra were calculated using the parameters summarized in Table **3.1**.

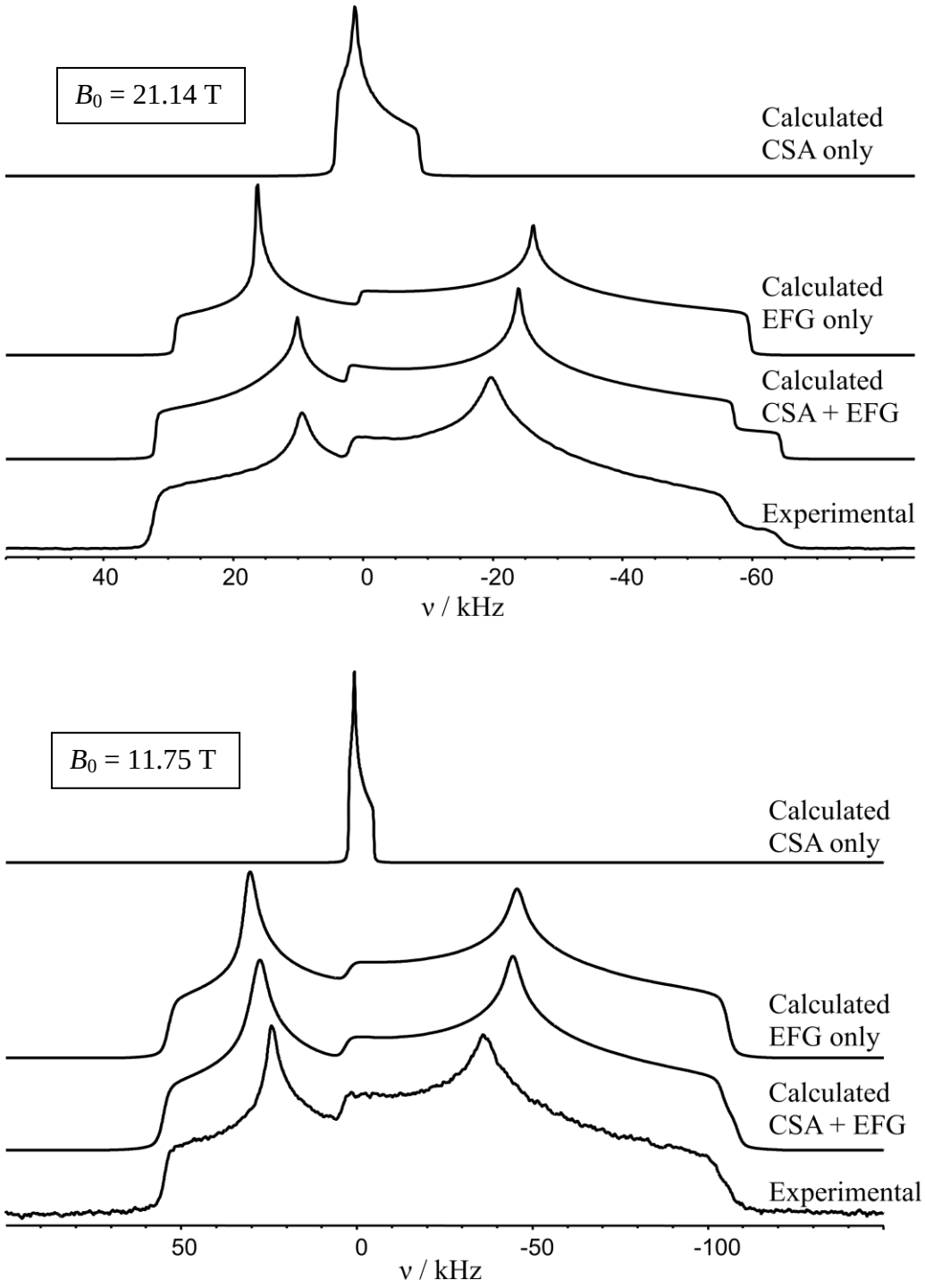

Figure 3.6 Experimental and calculated ^{69}Ga NMR spectra of stationary $Ga(thd)_3$ at 11.75 and 21.14 T. The simulated spectra were calculated using the parameters summarized in Table **3.1**.

3.4 Ga(trop)$_3$

The ^{71}Ga NMR spectra of Ga(trop)$_3$ at 21.14 T under MAS conditions is shown in Figure **3.7**. Preliminary fits of previously acquired data were performed by Dr. Guy Bernard, which were further refined in this study. As with previous MAS spectra, the spectrum was fit using Wsolids1, and the values $|C_Q(^{71}Ga)|$ = 10.98 ± 0.05 MHz, η_Q = 0.10 ± 0.01, and δ_{iso} = 106.0 ± 0.3 ppm were extracted. These agree reasonably well (within approximately 20 %) of the calculated C_Q obtained from CASTEP, and agree very well (within error) with the calculated value for η_Q of 0.096.

^{71}Ga and ^{69}Ga NMR spectra of stationary Ga(trop)$_3$ are shown in Figures **3.8** and **3.9**. Fits of these spectra were also performed, with $|C_Q(^{69}Ga)|$ determined from $|C_Q(^{71}Ga)|$ as previously described. Interestingly, the CASTEP calculations, as well as our own fits, suggest that the three Euler angles relating the CSA and EFG tensors are α = 0°, β = 90°, and γ = 0°. Note that some values of Euler angles will yield equivalent calculated spectra, such as α = 0° and α = 180°; thus, the CASTEP calculated Euler angles and those determined from the fitting procedure are in agreement. This indicates that the principal components δ_{11}, δ_{22} and δ_{33} are likely oriented parallel to eq_{zz}, eq_{yy}, and eq_{xx}, respectively.

Relative to the broadening of the CT caused by the quadrupolar interaction, the CSA broadening is fairly small in magnitude. The determined value for Ω of 45 ± 10 ppm agrees fairly well (nearly within error) to the CASTEP calculated value, but the minor influence of the CSA interaction on the overall powder pattern made it difficult to obtain an unambiguous value for κ. As

such, we report κ = -0.3 ± 0.2. The pseudo-octrahedral local GaO_6 environment of $Ga(trop)_3$ is more heavily distorted from a true local GaO_6 octahedral environment than it is in $Ga(acac)_3$. $Ga(trop)_3$[18] has O-Ga-O bond angles (ideally 90° for a perfect octahedron) ranging from 80.8°-95.3° compared to 88.0°-92.2° in $Ga(acac)_3$.[15] This is likely the reason for the larger C_Q and Ω values in $Ga(trop)_3$ compared to $Ga(acac)_3$.

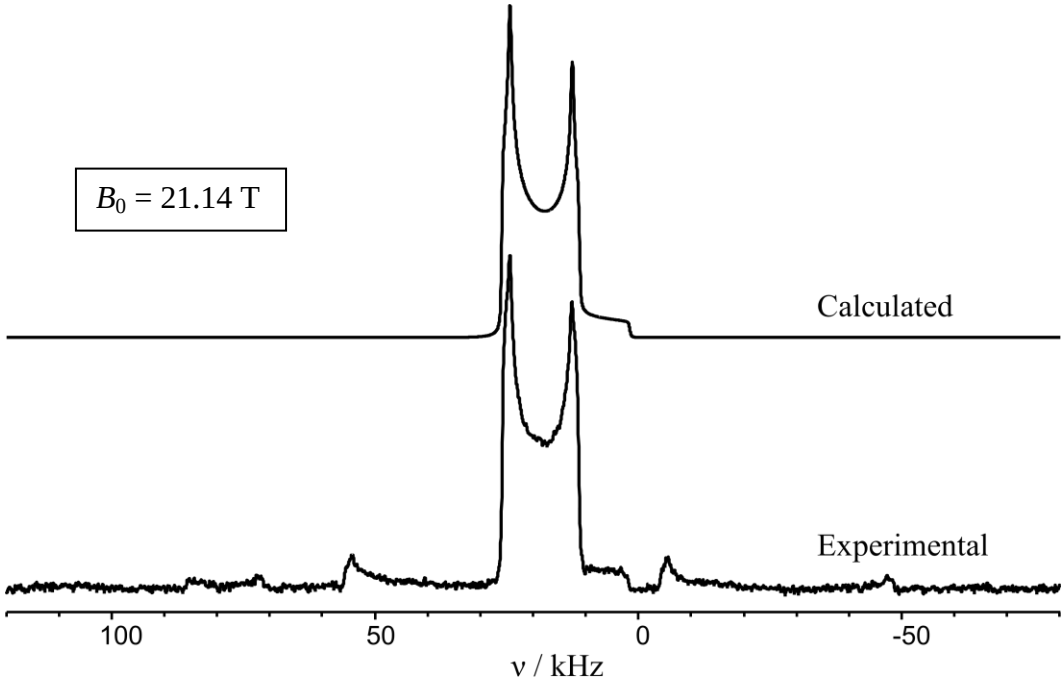

Figure 3.7 Experimental and calculated ^{71}Ga NMR spectra of $Ga(trop)_3$ under 30 kHz MAS at 21.14 T. The simulated spectrum was calculated using the parameters summarized in Table **3.1**. The peaks to either side of the central, high-intensity peak are spinning sidebands.

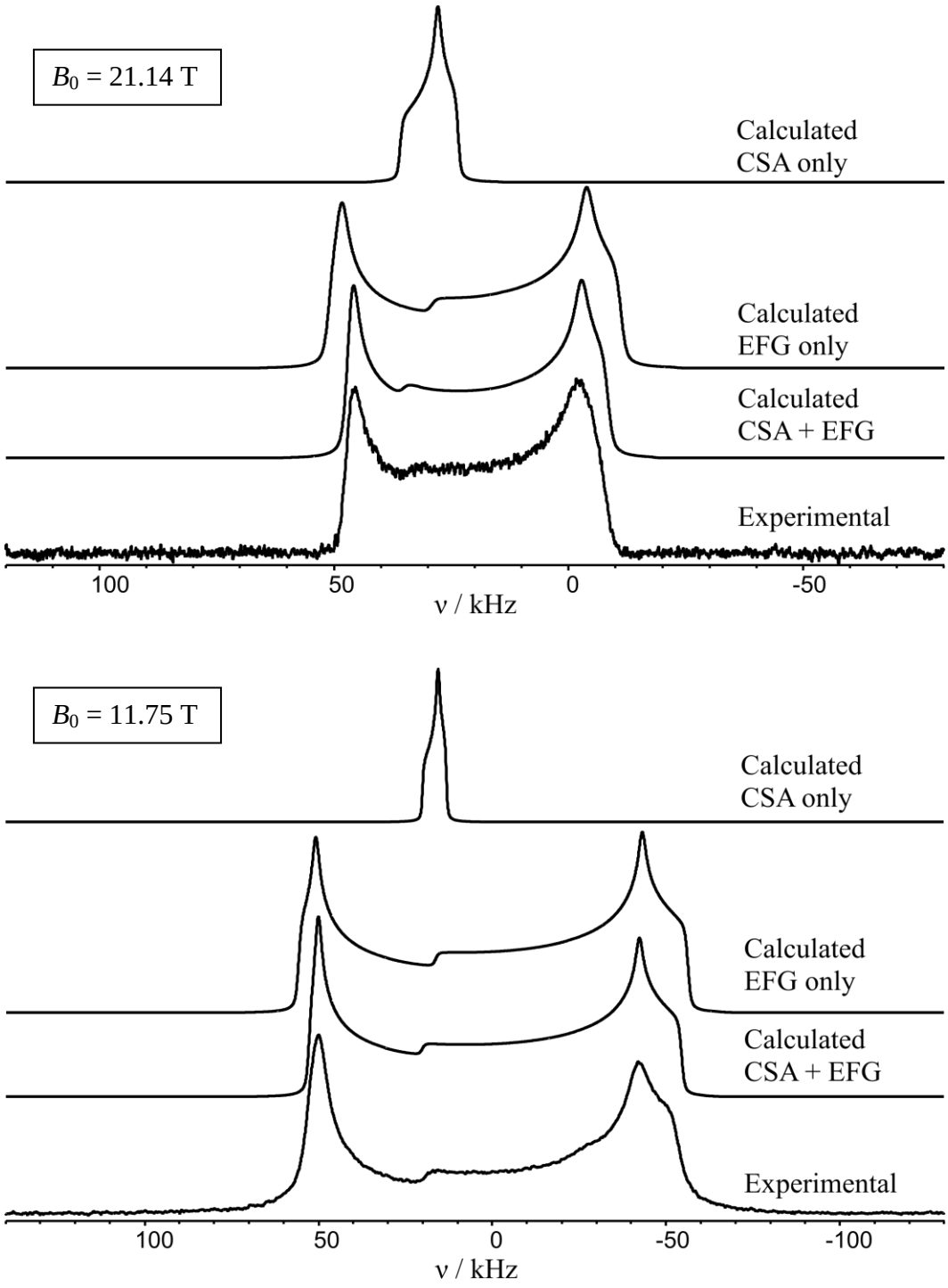

Figure 3.8 Experimental and calculated ^{71}Ga NMR spectra of stationary $Ga(trop)_3$ at 11.75 and 21.14 T. The simulated spectra were calculated using the parameters summarized in Table **3.1**.

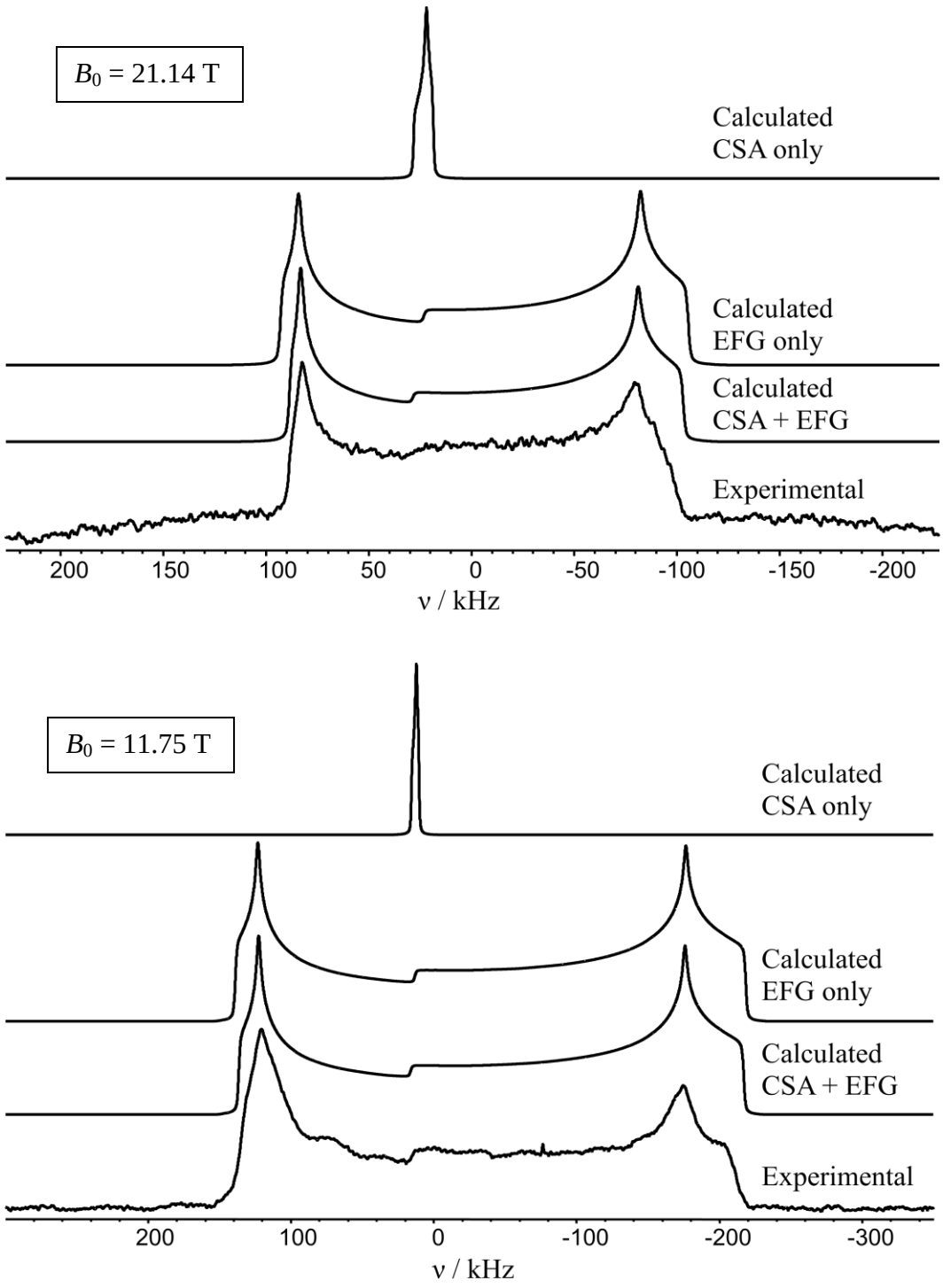

Figure 3.9 Experimental and calculated ^{69}Ga NMR spectra of stationary $Ga(trop)_3$ at 11.75 and 21.14 T. The simulated spectra were calculated using the parameters summarized in Table **3.1**.

3.5 $(NH_4)_3[Ga(cit)_2]\cdot 4H_2O$

The ^{71}Ga and ^{69}Ga NMR spectra of stationary $(NH_4)_3[Ga(cit)_2]\cdot 4H_2O$ are shown in Figures **3.10** and **3.11** respectively. This material exhibited by far the largest $|C_Q(^{71}Ga)|$ and $|C_Q(^{69}Ga)|$ out of the compounds studied here. In fact, the CT powder pattern of the ^{69}Ga NMR spectrum at 21.14 T is approximately 1.8 MHz in breadth. Since the CT powder patterns of the stationary samples were so broad, MAS was not practical in this case. Also, given the breadth of the spectrum at 21.14 T, a ^{69}Ga NMR spectrum of the complex at 11.75 T was not practical either, as it would have been (by Equation **1.18**) over 3 MHz in width. Such a spectrum would have likely required weeks to acquire.

Since MAS data was unavailable, fits of all NMR parameters were performed using the stationary spectra directly. Fortunately, several features of the obtained spectra facilitated this. First, the results of the CASTEP calculations were considered, and the appearances of calculated CT powder patterns using these results were examined. It was initially apparent that the CASTEP calculation had underestimated the magnitude of the quadrupolar coupling constants by slightly less than 30 %, as determined primarily by the breadth of the powder pattern. However, the remainder of the parameters seemed to yield a fairly close fit. The fit was refined by adjusting the parameter values, with particular attention paid to the effect of their values on the slight splitting in the high-frequency horn of the ^{71}Ga NMR spectrum at 21.14 T and the position of the shoulder in the centre of the powder pattern. Euler angles of $\alpha = 197 \pm 5°$, $\beta = 0 \pm 2°$, and $\gamma = 262 \pm 2°$ were determined, and equivalent angles of $\alpha = 17 \pm 5$ and $\gamma =$

82 ± 2° were found (spectra calculated with both sets of Euler angles were identical). The determined Euler angles and the CASTEP calculated angles agree within error (or just outside error in the case of β).

The determined values of η_Q = 0.48 ± 0.01, κ = 0.35 ± 0.10, and Ω = 260 ± 15 ppm also agree with the CASTEP results within error. The final determined quadrupolar coupling constant magnitudes were $|C_Q(^{71}Ga)|$ = 28.4 ± 0.5 MHz and $|C_Q(^{69}Ga)|$ = 45.0 ± 0.5 MHz. All parameters have been summarized in Table **3.1**. It should be noted that it is impossible to determine the sign of C_Q from the CT powder pattern of a quadrupolar nucleus in the absence of any effects other than CSA and quadrupolar coupling. However, the CASTEP results indicate negative C_Q values, and given the high magnitude of these coupling constants and the close match between calculated and experimentally determined parameters, we can confidently report that the gallium quadrupolar coupling constants for $(NH_4)_3[Ga(cit)_2]\cdot 4H_2O$ are $C_Q(^{71}Ga)$ = -28.4 ± 0.5 MHz and $C_Q(^{69}Ga)$ = -45.0 ± 0.5 MHz.

It is not surprising that $(NH_4)_3[Ga(cit)_2]\cdot 4H_2O$ has the largest C_Q and Ω values of the compounds studied. Given the fact that the gallium site is coordinated to two tridentate ligands (note that the ligand geometry demands a *fac* coordination scheme) rather than three bidentate ligands, the environment around the Ga is the most different from octahedral symmetry in $(NH_4)_3[Ga(cit)_2]\cdot 4H_2O$ compared to the environments of $Ga(acac)_3$, $Ga(thd)_3$, and $Ga(trop)_3$, which are closer to octahedral. This has almost certainly led to very strong shielding anisotropy and quadrupolar coupling in $(NH_4)_3[Ga(cit)_2]\cdot 4H_2O$.

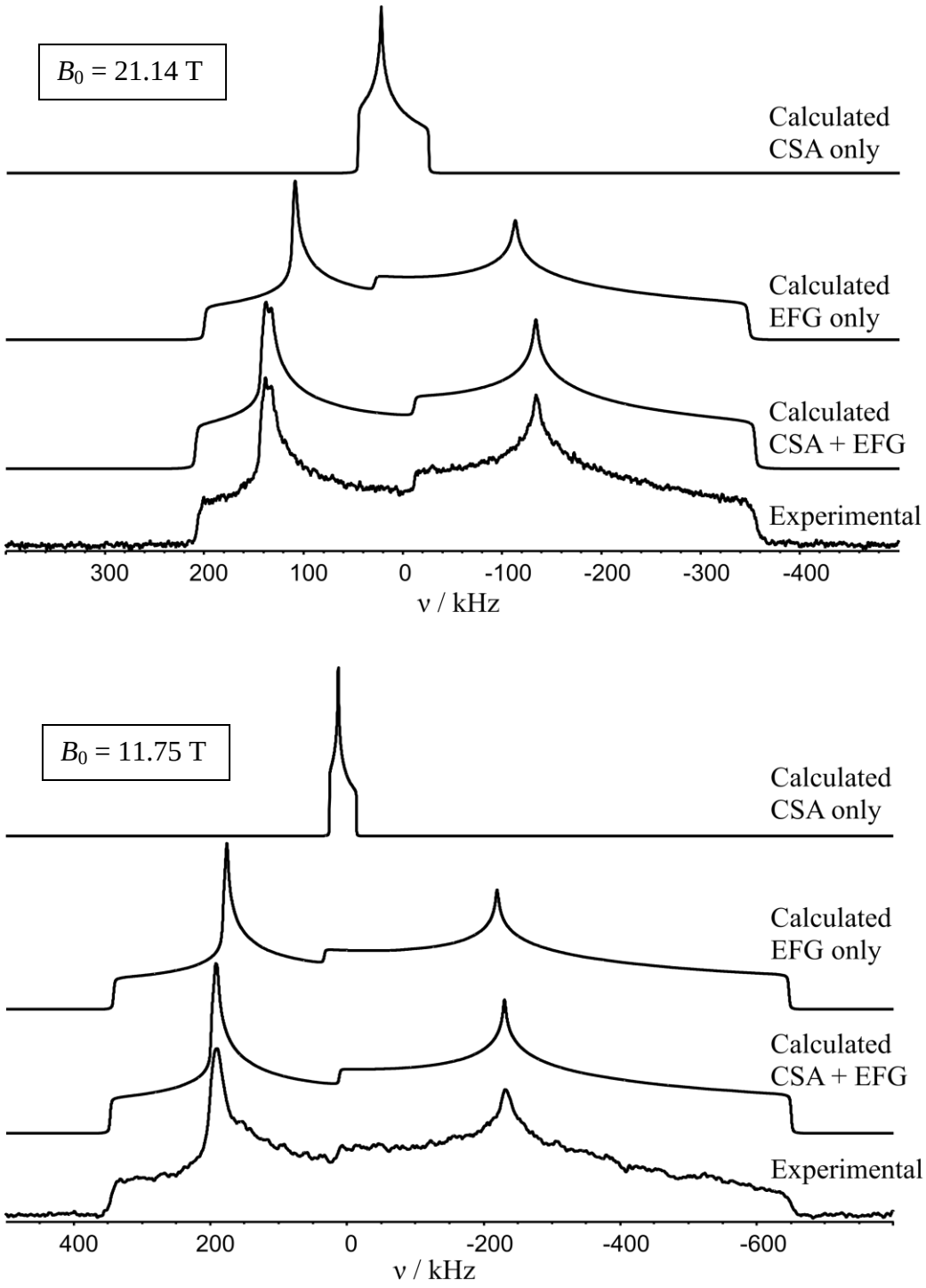

Figure 3.10 Experimental and calculated ^{71}Ga NMR spectra of stationary $(NH_4)_3[Ga(cit)_2]\cdot 4H_2O$ at 11.75 and 21.14 T. The simulated spectra were calculated using the parameters summarized in Table **3.1**.

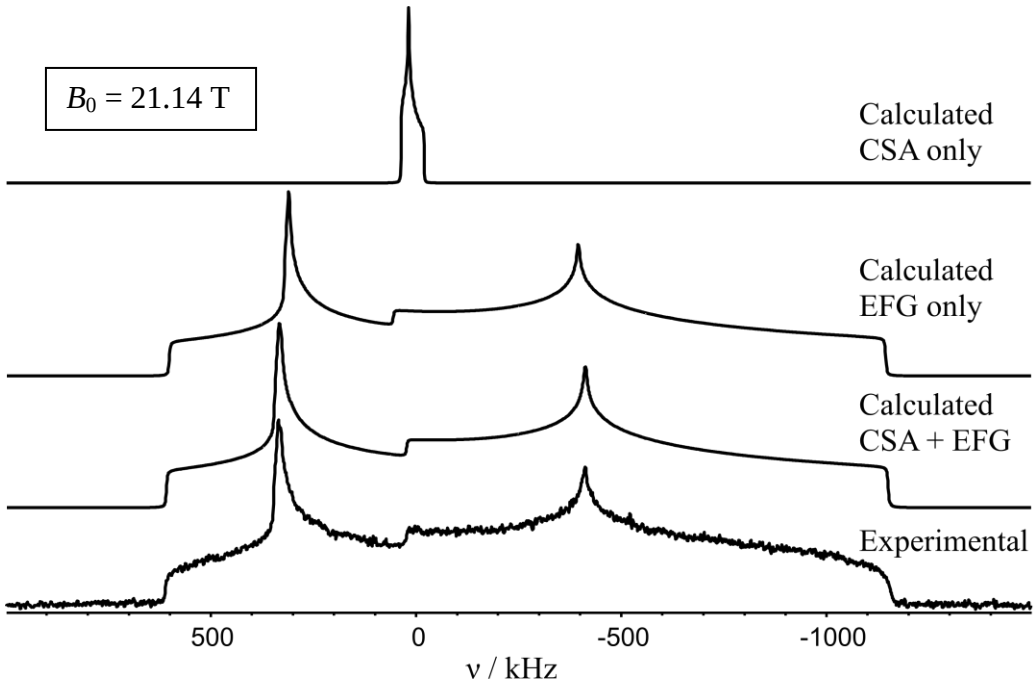

Figure 3.11 Experimental and calculated ^{69}Ga NMR spectra of stationary $(NH_4)_3[Ga(cit)_2]\cdot 4H_2O$ at 21.14 T. The simulated spectra were calculated using the parameters summarized in Table **3.1**.

3.6 Comparison of Results

Table **3.3** shows a comparison of the NMR parameters presented here with those reported[67,68] for other group-13 metal $M(acac)_3$ complexes, while Tables **3.4** and **3.5** show those for $M(trop)_3$ and $M(thd)_3$ respectively. A clear trend is evident; as one travels down the periodic table from Al to In, the magnitudes of the C_Q, δ_{iso}, and Ω all increase. One should note that the reason for the increase in C_Q is not simply due to differences in the quadrupole moments of the three nuclei. Rather, the largest component of the EFG tensor, eq_{zz}, increases by approximately a factor of 3 from the Al to Ga samples and approximately a factor of 2 from the Ga to In samples for the compounds studied. This makes sense since, in general, eq_{zz} depends on the expectation value of $<1/r^3>$, where r is the average distance between the nucleus and valence p electrons.[24] As one moves down a group, $<1/r^3>$ increases as the p electrons are drawn closer to the nucleus.[69] Relativistic effects serve to further enhance this trend.[24] In addition, the local spherical symmetry of closed-shell electrons can be perturbed by what is known as the Sternheimer antishielding factor, generally increasing the effect of eq_{zz}.[24] This factor accounts for the portion of the EFG at a nucleus caused by the ion's (in this case Ga^{3+}) electrons,[70] and as one travels down a group, it also tends to increase.

A correlation between ^{27}Al and ^{71}Ga chemical shifts has been previously reported.[71] While we do not observe strict adherence to the reported mathematical relationship between δ_{iso} for ^{71}Ga and ^{27}Al, we do observe a similar trend, with ^{71}Ga chemical shifts being on the order of 2.5 to 3.5 times greater than for ^{27}Al. This phenomenon, as well as the fact that the spans increase as one

travels down the group, can be explained on the basis of the paramagnetic component of magnetic shielding. This term is also dependent on $<1/r^3>$, and as such, the range of chemical shift values increases as one descends the periodic table.[24]

Table 3.3 Summary NMR properties for group-13 $M(acac)_3$ complexes.

	M = ^{27}Al	M = ^{71}Ga	M = ^{115}In
$\lvert C_Q \rvert$ / MHz	3.03 ± 0.01	6.62 ± 0.14	106 ± 2
η_Q	0.15 ± 0.01	0.16 ± 0.01	0.14 ± 0.05
δ_{iso} / ppm	0.0 ± 0.3	-10.4 ± 0.1	-35 ± 10
Ω / ppm	3.8 ± 0.3	<20	85 ± 15
κ	0.70 ± 0.03	≈ 0.7	-0.9 ± 0.1
α / °	90 ± 15	≈ 64	90 ± 20
β / °	90 ± 10	≈ 82	90 ± 5
γ / °	0 ± 30	≈ 4	0 ± 20
Reference	68	This Work	67

Table 3.4 Summary NMR properties for group-13 $M(trop)_3$ complexes.

	M = ^{27}Al	M = ^{71}Ga	M = ^{115}In
$\lvert C_Q \rvert$ / MHz	4.43 ± 0.01	10.98 ± 0.05	160 ± 2
η_Q	0.08 ± 0.02	0.10 ± 0.01	0[a]
δ_{iso} / ppm	36.6 ± 0.2	106.0 ± 0.3	160 ± 20
Ω / ppm	9.0 ± 0.3	45 ± 10	180 ± 30
κ	-0.25 ± 0.05	-0.3 ± 0.2	-1.00[a]
α / °	90 ± 5	0 ± 10	90[a]
β / °	81 ± 2	90 ± 5	90[a]
γ / °	7 ± 2	0 ± 20	0[a]
Reference	68	This Work	67

[a] These values are restricted by the crystallographic symmetry at the metal site. The EFG and CSA tensors are axially symmetric.

Table 3.5 Summary NMR properties for group-13 $M(thd)_3$ complexes.

	M = ^{27}Al	M = ^{71}Ga
$\lvert C_Q \rvert$ / MHz	3.23 ± 0.02	6.50 ± 0.05
η_Q	0.10 ± 0.01	0.40 ± 0.02
δ_{iso} / ppm	1.5 ± 0.3	-5.5 ± 0.5
Ω / ppm	6.7 ± 0.5	60 ± 15
κ	0.4 ± 0.1	0.54 ± 0.20
α / °	90 ± 25	114 ± 20
β / °	90 ± 10	70 ± 20
γ / °	0 ± 30	120 ± 20
Reference	68	This Work

Chapter 4: Conclusions

^{69}Ga and ^{71}Ga SS NMR spectra were acquired for $Ga(acac)_3$, $Ga(thd)_3$, $Ga(trop)_3$, and $(NH_4)_3[Ga(cit)_2]\cdot 4H_2O$ at 11.75 and 21.14 T. Stationary and MAS spectra were fit to calculated spectra to extract the NMR parameters of interest, namely C_Q, η_Q, δ_{iso}, Ω, and κ, as well as the Euler angles relating the CSA and EFG tensors, α, β, and γ. Results were compared with those obtained through CASTEP calculations, and generally, the results were in qualitative agreement, with the exception of $Ga(thd)_3$. For that material, no crystal structure data has been reported, and as such, the calculated parameters obtained using a theoretical molecular structure do not appear to closely reflect those obtained experimentally.

In summary, the trends we observe in our data, as well as the comparison of our data to other group-13 metal SS NMR studies, agree as expected with the literature. ^{69}Ga and ^{71}Ga SS NMR spectroscopy are powerful tools available to chemists and materials scientists, and were successfully used to characterize the gallium environments in the six-coordinate gallium-oxygen complexes investigated here. It has been shown that ^{69}Ga and ^{71}Ga SS NMR studies are practical and worthwhile methods of studying the properties of solid gallium materials.

This work could be improved through several avenues. The use of stronger external magnetic fields could help elucidate the CSA tensor properties and Euler angles for $Ga(acac)_3$. Also, more accurate calculations, though time consuming, could further help refine the NMR parameters for all compounds studied, especially if a reliable crystal structure could be obtained for $Ga(thd)_3$.

Single-crystal NMR studies of the compounds investivated here might also yield more definitive NMR parameter values, especially for the Euler angles. Further NMR studies of other gallium compounds will lead to a better understanding of ^{69}Ga and ^{71}Ga NMR properties, too. The six-coordinate gallium maltolate and gallium oxalate species in particular might be worth investigating.[2]

References

1. *The Group 13 Metals Aluminium, Gallium, Indium and Thallium: Chemical Patterns and Peculiarities.* Aldridge, S.; Downs, A.J., Eds.; John Wiley & Sons Ltd.: Chichester, **2011**.
2. Bandoli, G.; Dolmella, A.; Tisato, F.; Porchia, M.; Refosco, F. *Coord. Chem. Rev.* **2009**, *253*, 56-77.
3. *NMR Crystallography*; Harris, R. K.; Wasylishen, R. E.; Duer, M. J., Eds.; John Wiley & Sons Ltd.: Chichester, **2009**.
4. Ash, J.T.; Grandinetti, P.J. *Magn. Reson. Chem.* **2006**, *44*, 823-831.
5. Chapman, R.P.; Bryce, D.L. *Phys. Chem. Chem. Phys.* **2009**, *11*, 6987-6998.
6. Volkringer, C.; Loiseau, R.; Ferey, G.; Morais, C.M.; Taulelle, F.; Montouillout, V.; Massiot, D. *Microporous Mesoporous Mater.*, **2007**, *105*, 111-117.
7. Hajjar, R.; Volkringer, C.; Loiseau, T.; Guillou, N.; Marrot, J.; Ferey, G.; Margiolaki, I.; Fink, G.; Morais, C.; Taulelle, F. *Chem. Mater.*, **2011**, *23*, 39-47.
8. Chen, F; Ma, G.; Bernard, G.M.; Wasylishen, R.E.; Cavell, R.G.; McDonald, R.; Ferguson, M.J. *Chem. Eur. J.*, **2013**, *19, 2826-2838.*
9. Haouas, M.; Martineau, C.; Taulelle, F. "Quadrupolar NMR of Nanoporous Materials" in *NMR of Quadrupolar Nuclei in Solid Materials*; Wasylishen, R. E.; Ashbrook, S. E.; Wimperis, S., Eds.; John Wiley & Sons Ltd.: Chichester, **2012**; p 371-386.

10. Harris, R.K.; Becker, E.D.; de Menezes, S.M.C.; Goodfellow, R.; Granger, P. *Pure Appl. Chem.* **2001**, *73*, 1795-1818.
11. Pyykkö, P. *Mol. Phys.* **2008**, *106*, 1965-1974.
12. Tang, J.A.; O'Dell, L.A.; Aguiar, P.M.; Lucier, B.E.G.; Sakellariou, D.; Schurko, R.W. *Chem. Phys Lett.* **2008**, *466*, 227-234.
13. O'Dell, L.A.; Schurko, R.W. *Chem. Phys. Lett.* **2008**, *464*, 97-102.
14. Bandoli, G.; Dolmella, A.; Tisato, F.; Porchia, M.; Refosco, F. *Coord. Chem. Rev.* **2009**, *253*, 56-77.
15. Dymock, K.; Palenik, G.J. *Acta Crystallog. B.* **1974**, *30*, 1364-1366.
16. Chae, S.-A.; Han, O.H.; Jung, W.-S. *Bull. Korean Chem. Soc.* **2009**, *30*, 2762-2764.
17. Belova, N.V.; Sliznev, V.V.; Zhukova, T.A.; Girichev, G.V. *Comp. Theor. Chem.* **2011**, *967*, 199-205.
18. Nepveu, F.; Jasanada, F.; Walz, L. *Inorg. Chim. Acta*. **1993**, *211*, 141-147.
19. Hawkes, G.E.; O'Brien, P.; Salacinski, H.; Motevalli, M.; Abrahams, I. *Eur. J. Inorg. Chem.* **2001**, 1005-1011.
20. O'Brien, P.; Salacinski, H.; Motevalli, M. *J. Am. Chem. Soc.* **1997**, *119*, 12695-12696.
21. Jackson, G.E.; ByrneM.J. *J. Nucl. Med.* **1996**, *37*, 1013-1016.
22. Harris, R.K. *Nuclear Magnetic Resonance Sepctroscopy: A Physicochemical View*. Longman: Durham, **1983**. 260p.

23. Hore, P.J. *Oxford Chemistry Primers: Nuclear Magnetic Resonaonce*. Oxford University Press: New York, **1995**. 90p.
24. Slichter, C. P. *Principles of Magnetic Resonace, 2nd Ed.*; Springer: New York, **1978**.
25. Akitt, J. W.; Mann, B. E. *NMR and Chemistry: An Introduction to Modern NMR Spectroscopy*; 4th ed.; Stanley Thornes: Cheltenham, U.K., **2000**.
26. Harris, R. K.; Becker, E. D.; De Menezes, S. M. C.; Granger, P.; Hoffman, R. E.; Zilm, K. W. *Pure Appl. Chem.* **2008**, *80*, 59-84.
27. Anet, F.A.; O'Leary, D.J. *Concept Magnetic Res.* **1991**, *3*, 193-214.
28. Anet, F.A.; O'Leary, D.J. *Concept Magnetic Res.* **1992**, *4*, 35-52.
29. Wasylishen, R. E.; Bernard, G. M. in *Comprehensive Organometalic Chemistry;* Mingos, D. M. P., Crabtree, R. H., Eds. Elsevier: Oxford, **2007.** Vol. I, p 451-482.
30. Herzfeld, J.; Berger, A.E. *J. Chem. Phys.* **1980**, *73*, 6021-6030.
31. Mason, J. *Solid State Nucl. Magn. Reson.* **1993**, *2*, 285-288.
32. Eichele, K. WSolids1 ver. 1.20.15; Universität Tübingen, **2011**.
33. Bryce, D.L. "Tensor Interplay" in *NMR Crystallogrpahy*; Harris, R. K.; Wasylishen, R. E.; Duer, M. J., Eds.; John Wiley & Sons Ltd.: Chichester, **2009**; p 289-301.
34. Bryce, D. L.; Wasylishen, R. E. "Quadrupolar Nuclei in Solids: Influence of Different Interactions on Spectra" in *NMR of Quadrupolar Nuclei in Solid Materials*; Wasylishen, R. E.; Ashbrook, S. E.; Wimperis, S., Eds.; John Wiley & Sons Ltd.: Chichester, **2012**; p 63-74.

35. Man, P.P. “Quadrupolar Interactions” in *NMR of Quadrupolar Nuclei in Solid Materials*; Wasylishen, R. E.; Ashbrook, S. E.; Wimperis, S., Eds.; John Wiley & Sons Ltd.: Chichester, **2012**; p 3-16.
36. Abragam, A. *The Principles of Nuclear Magnetism*. Oxford University Press: **1961**. 599 p.
37. Amoureux, J.-P.; Fernandez, C.; Granger, P. *NATO ASI Ser., Ser. C.* **1990**, *322*, 409-424.
38. *NMR of Quadrupolar Nuclei in Solid Materials*; Wasylishen, R. E.; Ashbrook, S. E.; Wimperis, S., Eds.; John Wiley & Sons Ltd.: Chichester, **2012**.
39. Chmelka, B.F.; Zwanziger, J.W. *NMR-Basic Princ. Prog.* **1994**, *33*, 79-124.
40. Samoson, A.; Kundla, E.; Lippmaa, E. *J. Magn. Reson.* **1982**, *49*, 350-357.
41. Schmidt-Rohr, K.; Spiess, H.W. “Appendix B: Rotations and Euler Angles” in *Miltidimensional Solid-State NMR and Polymers*. Academic Press Ltd.: London, **1994**.; p. 444-452.
42. Ashbrook, S.E.; Wimperis, S. “Quadrupolar Coupling: An Introduction and Crystallographic Aspects” in *NMR of Quadrupolar Nuclei in Solid Materials*; Wasylishen, R. E.; Ashbrook, S. E.; Wimperis, S., Eds.; John Wiley & Sons Ltd.: Chichester, **2012**; p 45-61.
43. Kodweiss, J.; Lutz, O.; Messner, W.; Mohn, K.R.; Nolle, A.; Stütz, B.; Zepf, D. *J. Magn. Reson*. **1981**, *43*, 495.

44. Earl, W.L.; VanderHart, D. L. *J. Magn. Reson.* **1982**, *48*, 35-54.

45. Schurko, R.W. "Acquisition of Wideline Solid-State NMR Spectra of Quadrupolar Nuclei" in *NMR of Quadrupolar Nuclei in Solid Materials*; Wasylishen, R. E.; Ashbrook, S. E.; Wimperis, S., Eds.; John Wiley & Sons Ltd.: Chichester, **2012**; p 77-93.

46. Vega, A.J. "Quadrupolar Nuclei in Solids" in *NMR of Quadrupolar Nuclei in Solid Materials*; Wasylishen, R. E.; Ashbrook, S. E.; Wimperis, S., Eds.; John Wiley & Sons Ltd.: Chichester, **2012**; p 17-44.

47. Spiess, H.W.; Sillescu, H. *J. Magn. Reson.* **1981**, *42*, 381-389.

48. Davis, J.H.; Jeffrey, K.R.; Bloom, M.; Valic, M.I.; Higgs, T.P. *Chem. Phys. Lett.* **1976**, *42*, 390-394.

49. Bodart, P.R.; Amoureux, J.-P.; Dumazy, Y.; Lefort, R. *Mol. Phys.* **200**, *98*, 1545-1551.

50. Andrew, E.R.; Bradbury, A.; Eades, R.G. *Nature*. **1958**, *182*, 1659.

51. Lowe, I.J. *Phys. Rev. Lett.* **1959**, *2*, 285-287.

52. Nagayama, K.; Bachmann, P.; Wuethrich, K.; Ernst, R.R. *J. Magn. Reson.* **1978**, *31*, 133-148.

53. Bluemich, B.; Ziessow, D. *J. Magn. Reson.* **1982**, *49*, 151-154.

54. Lipton, A.S.; Wright, T.A.; Bowman, M.K.; Reger, D.L.; Ellis, P.D. *J. Am. Chem. Soc.* **2002**, *124*, 5850-5860.

55. Kupče, E.; Freeman, R. *J. Magn. Reson. Ser. A.* **1995**, *115*, 273-276.

56. Kupče, E.; Freeman, R. *J. Magn. Reson. Ser. A.* **1995**, *117*, 246-256.

57. Clark, S.J.; Segall, M.D.; Pickard, C.J.; Hasnip, P.J.; Probert, M.J.; Refson, K.; Payne, M.C. *Z. Kristallogr.* **2005**, *220*, 567-570.

58. Pickard, C.J.; Mauri, F. *Phys. Rev. B.* **2001**, *63*, 245101.

59. Yates, J.R.; Pickard, C.J.; Mauri, F. *Phys. Rev. B.* **2007**, *76*, 024401.

60. Profeta, M.; Mauri, F.; Pickard, C.J. *J. Am. Chem. Soc.* **2003**, *125*, 541-548.

61. Adiga, S.; Aebi, D.; Bryce, D.L.; Dicaire, N. EFGShield ver. 3. University of Ottawa, **2005-2011**.

62. Adiga, S.; Aebi, D.; Bryce, D.L. *Can. J. Chem.* **2007**, *85*, 496-505.

63. Bonhomme, C.; Gervais, C.; Babonneau, F.; Coelho, C.; Pourpoint, F.; Azais, T.; Ashbrook, S.E.; Griffin, J.M.; Yates, J. R.; Mauri, F.; Pickard, C.J. *Chem. Rev.* **2012**, *112*, 5733-5779.

64. Charpentier, T. *Solid State Nucl. Magn. Reson.* **2011**, *40*, 1-20.

65. Jaeger, F.M. *P. K. Ned. Akad. Wetensc.* **1930**, *33*, 280-283.

66. Dechter, J.J.; Henriksson, U.; Kowalewski, J.; Nilsson, A.-C. *J. Magn. Reson.* **1982**, *48*, 503-511.

67. Chen, F.; Ma, G.; Cavell, R.G.; Terskikh, V.V.; Wasylishen, R.E. *Chem. Commun.* **2008**, 5933-5935.

68. Schurko, R.W.; Wasylishen, R.E.; Foerster, H. *J. Phys. Chem. A.* **1998**, *102*, 9750-9760.

69. Jameson, C.J.; Mason, J. "Chapter 3: The Chemical Shift" in *Multinuclear NMR;* Mason, J. Ed.;Plenum Press: New York, **1987**; p 51-88.

70. Schmidt, P.C.; Sen, K.D.; Das, T.P.; Weiss, A. *Phys. Rev. B.* **1980**, *22*, 4167-4179.

71. Bradley, S.M.; Howe, R.F.; Kydd, R.A. *Magn.Reson Chem.* **1993**, *31*, 883-886.

Appendix 1: List of Publications by the Author

1. **Feland, B.C**.; Bernard, G.M.; Wasylishen, R.E. "A Solid-State NMR Investigation of the Colossal Expansion Material $Ag_3Co(CN)_6$." *Can. J. Chem.* **2012**, *90*, 891-901.
2. Lane, E.M.; Chapp, T.W.; Hughes, R.P.; Glueck, D.S.; **Feland, B.C.**; Bernard, G.M.; Wasylishen, R.E; Rheingold, A.L. "Synthesis of Gold Phosphido Complexes Derived from Bis(secondary) Phosphines. Structure of Tetrameric $[Au(MesP(CH_2)_3PMes)Au]_4$." *Inorganic Chemistry*. **2010**, *49*, 3950-3957.
3. Halse, M.E.; Callaghan, P.T.; **Feland, B.C.**; Wasylishen, R.E. "Quantitative Analysis of Earth's Field NMR Spectra of Strongly-Coupled Heteronuclear Systems." *Journal of Magnetic Resonance*. **2009**, *200*, 88-94.

Appendix 2: Skyline Projections

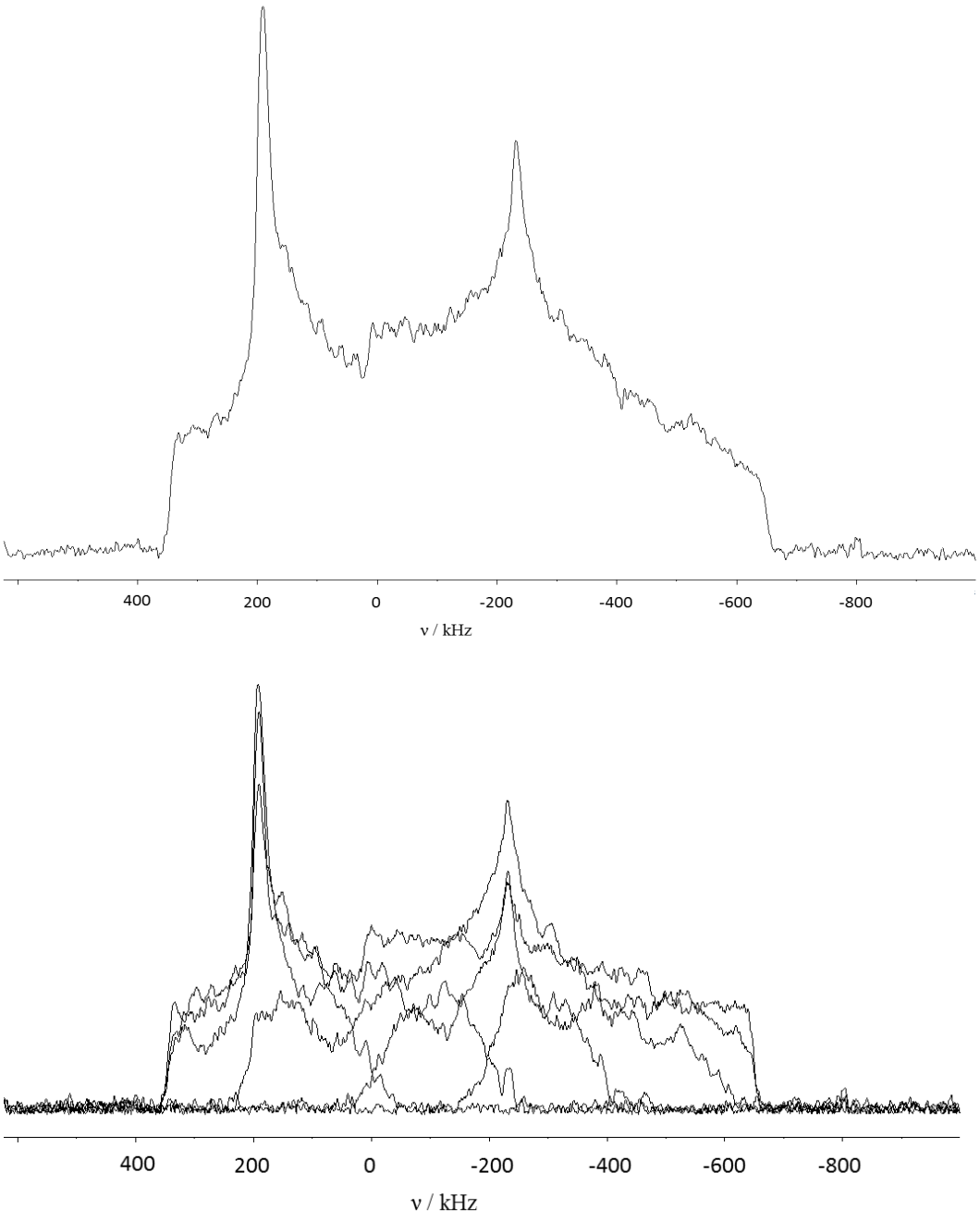

Figure A2 An example of a good approximation of a skyline projection. Shown is the ^{71}Ga SS NMR spectrum of stationary $(NH_4)_3[Ga(cit)_2]\cdot 4H_2O$ at 11.75 T obtained in 6 windows with WURST-echo pulses in transmitter offset steps of 200 kHz, relative to 0 ppm, from +400 to -600 kHz. All six windows are displayed superimposed (lower trace), and the sum of the six windows is shown (upper trace).